2014

Elastic models for nonlinear response of rigid passive piles

Wei Dong Guo
University of Wollongong, wdguo@uow.edu.au

Elastic models for nonlinear response of rigid passive piles

Abstract

Recent study indicates that the response of rigid passive piles is dominated by elastic pile–soil interaction and may be estimated using theory for lateral piles. The difference lies in that passive piles normally are associated with a large scatter of the ratio of maximum bending moment over maximum shear force and induce a limiting pressure that is ~1/3 that on laterally loaded piles. This disparity prompts this study.

This paper proposes pressure-based pile–soil models and develops their associated solutions to capture response of rigid piles subjected to soil movement. The impact of soil movement was encapsulated into a power-law distributed loading over a sliding depth, and load transfer model was adopted to mimic the pile–soil interaction. The solutions are presented in explicit expressions and can be readily obtained. They are capable of capturing responses of model piles in a sliding soil owing to the impact of sliding depth and relative strength between sliding and stable layer on limiting force prior to ultimate state. In comparison with available solutions for ultimate state, this study reveals the 1/3 limiting pressure (of the active piles) on passive piles was induced by elastic interaction. The current models employing distributed pressure for moving soil are more pertinent to passive piles (rather than plastic soil flow). An example calculation against instrumented model piles is provided, which demonstrates the accuracy of the current solutions for design slope stabilising piles.

Keywords

nonlinear, models, elastic, piles, response, rigid, passive

Disciplines

Engineering | Science and Technology Studies

Publication Details

Guo, W. D. (2014). Elastic models for nonlinear response of rigid passive piles. International Journal for Numerical and Analytical Methods in Geomechanics, 38 (18), 1969-1989.

Date revised: 18 September, 2013; 5 February, 2014; 10 March, 2014

Title: Elastic Models for Nonlinear Response of Rigid Passive Piles

Wei Dong Guo

Affiliation and address:
Associate Professor Wei Dong Guo
School of Civil, Mining & Environmental Engineering
University of Wollongong, NSW 2522, Australia
Email: camsaweidguo@lycos.com; wdguo@uow.edu.au
Tel: (61-2) 4221 3036

Number of tables: 5
Number of figures: 16

Key words: piles, closed-form solutions, soil movement, soil-structure interaction

ABSTRACT

Recent study indicates response of rigid passive piles is dominated by elastic pile-soil interaction, and may be estimated using theory for lateral piles. The difference lies in that passive piles normally are associated with a large scatter of the ratio of maximum bending moment over maximum shear force; and induce a limiting pressure that is ~ 1/3 that on laterally loaded piles. This disparity prompts this study.

This paper proposes pressure-based pile-soil models and develops their associated solutions to capture response of rigid piles subjected to soil movement. The impact of soil movement was encapsulated into a power-law distributed loading over a sliding depth, and load transfer model was adopted to mimic the piles-soil interaction. The solutions are presented in explicit expressions and can be readily obtained. They are capable of capturing responses of model piles in a sliding soil owing to the impact of sliding depth and relative strength between sliding and stable layer on limiting force prior to ultimate state. In comparison with available solutions for ultimate state, this study reveals the 1/3 limiting pressure (of the active piles) on passive piles was induced by elastic interaction. The current models employing distributed pressure for moving soil are more pertinent to passive piles (rather than plastic soil flow). An example calculation against instrumented model piles is provided, which demonstrates the accuracy of the current solutions for design slope stabilising piles.

Key words: passive piles, soil-structure interaction, closed-form solutions, slope stabilization

1 INTRODUCTION

Piles are often subjected to passive loading. Passive piles are largely well modelled using rigid pile-soil interaction in sliding layer as noted in slope-stabilising piles [1], or in piles subjected to lateral spreading [2-4]. Recent study indicates response of rigid passive piles is dominated by elastic pile-soil interaction [5], and may be modelled using theory for lateral piles but for the following discrepancies: A measured $M_m/(T_mL)$ ratio of 0.10~0.43 (M_m, T_m = maximum bending moment and shear force, respectively) from model passive piles compared to elastic solutions of 0.148~0.26 for lateral piles [6-7]. A deduced limiting force per unit length of (2.5~4) $s_u d$ (s_u = undrained shear strength, d = pile diameter) from measured response of passive piles in clay against the upper bound of (9.14~11.94)$s_u d$ for plastic flow [8]. The disparity between passive and lateral piles prompts this study on developing new models and solutions to mimic the response of passive piles.

Elastic solutions for laterally loaded piles [9] are utilised successfully to predict response of some passive piles [5]. The prediction utilises a concentrated thrust P (at sliding depth) gained from measured data or ultimate force per unit length (p_u) to model the impact of soil movement. The p_u-based model well captures the response of flexible piles using the equivalent concentrated thrust P at around sliding depth [1]. However, the use of the thrust cannot well capture the response of passive rigid piles. To resolve the issue, in this paper, new pressure based models are proposed, from which elastic solutions were developed. The impact of soil movement on piles is modelled by a distributed load exhibiting power-law increase with depth over sliding depth (for a single layer), or a uniformly distributed load over sliding layer (for two-layered soil), respectively. The solutions are presented in closed-form

expressions for calculating maximum bending moment M_m, shear force T_m, and their respective depths z_m, z_{mt} and for predicting profiles of shear force, bending moment, and deflection, etc. The solutions are compared with available plastic-state solutions (to reveal impact of progressive soil movement), and boundary element method (BEM) solutions (to check the accuracy). They are elaborated through an example calculation for model test piles.

2 SOLUTIONS FOR RIGID PILES IN MOVING SOIL

Figure 1 shows a rigid pile embedded in a moving soil to a depth of L_s. The movement has a magnitude of w_s at ground surface, and follows a uniform, or an inverse triangular variation with depth; or has a movement w_s at certain depth for an arc variation with depth. The impact of the moving soil on the piles may be mimicked by the corresponding distributed load p on the pile (termed herein as p-based model) shown in Figure 2. This resembles the ultimate-state solutions using a uniform force per unit length of p and mp (m = a multiplier) on the pile in the sliding and stable layer, respectively [10]. More specifically, the p-based pile-soil interaction models are underpinned by the following hypotheses, in the context of load transfer model [11]:

- The pile-soil interaction is modelled by a series of elastic springs along the pile shaft (Note shear force at the pile tip is ignored).
- Each spring has a constant coefficient of subgrade reaction k_s, regardless of depth (single layer); or has a constant k_s for sliding layer (to a depth L_s) and mk_s for stable layer (2-layer case);
- The pile has a linear variation in deflection with depth and a displacement –dependent on-pile force profile (with a specific upper limit).

- The distributed loading over the depth between *b* and *c* on a single pile [see Figure 2(a)-(c)] is expressed by (a) A uniform loading p (= $A_r z^n$, A_r = gradient [FL^{-1-n}], z = depth [L], n = 0); (b) A linearly increasing loading p (= $A_r z^n$, n = 1.0); or (c) A power-law increase p with depth ($p = A_r z^n$, n = 0 ~1.7). The distributed loading is uniform to a depth c in the sliding layer (see Figure 3a) for a 2-layer soil.

As mentioned early, the impact of sliding soil was also encapsulated into a concentrated thrust at sliding level [Figure 3(b)]. The associted solutions work well in certain circumstance [6] [1].

Next explicit solutions are developed for each p-based model; and for a uniform loading p on piles in a sliding soil (a two-layered soil), respectively. The solutions are all presented in closed-form expressions to facilitate calculation of maximum bending moment M_m, shear force T_m, and depth of maximum bending moment z_m. They are used to explore the impact of the p profile on pile response, and identify the difference from those caused by a concentrated thrust located at depth a (P-based model).

2.1 Solutions for $p = A_r z^n$ (Passive movement in a single layer)

A rigid pile is embedded in a single layered soil. In light the p-based model, the moving soil exerts a power-law increase force per unit length p on the pile with $p = A_r z^n$. The p spreads over a depth between b and c [see Figure 2], with n = 0 for a uniform movement, n = 1 for an inverse triangular soil movement, and other n for a parabolic movement, respectively. The elastic pile-soil interaction is characterised by a uniform coefficient of subgrade reaction k_s [FL^{-2}], and an induced force per unit length $p(z)$ [= $k_s w(z)$] [FL^{-1}]. The pile deflection at depth z, $w(z)$ is written as follows:

$$w(z) = (\overline{\omega}_r \overline{z} + \overline{w}_g)\frac{A_r L^n}{k_s} \quad (1)$$

where $\overline{\omega}_r$ [= $w'(z)k_s/(A_r L^{n-1})$], normalised rotation; $\overline{w}_g$ [= $w_g k_s/(A_r L^n)$], normalised displacement; $w'(z)$ = pile rotation (a constant along the rigid pile length), and w_g = pile-displacement at ground level. Note that the normalised $\overline{\omega}_r$ and $\overline{w}_g$ actually alter with the p profile (via A_r and n). In light of force and moment equilibrium, the solutions for the pile were deduced using Equation (1) for the distributed p profile with n = 0, 1, and other values. The profile of the shear force at loading zone (at depths b through c with subscript i = 2) and non-loading zone (i.e. without loading at depths *0* through b, and c through L with subscript i = 1 and 3) are also deduced. The maximum bending moment and its depth in loading and non-loading depth are summarised in Table 1, for a constant ultimate force per unit length p over the depths b through c [see Figure 2(a)]; and in Table 2 for a linear increase p [n = 1, see Figure 2(b)]. The profiles of displacement, shear force, and bending moment are provided in Table 3 for a power-law increase p [= $A_r z^n$, see Figure 2(c)] on the pile, respectively.

For instance, given a linear increase p (n = 1) [see Figure 2(a)], the solutions are as follows:

$$\overline{T}_1(\overline{z}) = \frac{1}{2}\overline{\omega}_r \overline{z}^2 + \overline{z}\overline{w}_g \qquad (\overline{z} < \overline{b}) \quad (2a)$$

$$\overline{T}_2(\overline{z}) = \frac{1}{2}(\overline{\omega}_r - 1)\overline{z}^2 + \overline{z}\overline{w}_g + \frac{1}{2}\overline{b}^2 \qquad (\overline{b} \le \overline{z} < \overline{c}) \quad (2b)$$

$$\overline{T}_3(\overline{z}) = \frac{1}{2}\overline{\omega}_r \overline{z}^2 + \overline{z}\overline{w}_g + \frac{1}{2}(\overline{b}^2 - \overline{c}^2) \qquad (\overline{c} \le \overline{z} \le 1) \quad (2c)$$

$$\overline{M}_1(\overline{z}) = \frac{\overline{\omega}_r \overline{z}^3}{6} + \frac{\overline{w}_g}{2}\overline{z}^2 \qquad (\overline{z} < \overline{b}) \quad (3a)$$

$$\overline{M}_2(\overline{z}) = \frac{(-1 + \overline{\omega}_r)\overline{z}^3}{6} + \frac{\overline{w}_g}{2}\overline{z}^2 + \frac{\overline{b}^2}{2}\overline{z} - \frac{\overline{b}^3}{3} \qquad (\overline{b} \le \overline{z} < \overline{c}) \quad (3b)$$

$$\overline{M}_3(\bar{z}) = \frac{\overline{\omega}_r}{6}\bar{z}^3 + \frac{\overline{w}_g}{2}\bar{z}^2 + \frac{(\bar{b}^2 - \bar{c}^2)}{2}\bar{z} + \frac{(\bar{c}^3 - \bar{b}^3)}{3} \quad (\bar{c} \le \bar{z} \le 1) \tag{3c}$$

where $\overline{T}_i(\bar{z}) = T_i(z)/(A_r L^2)$, $\overline{M}_i(\bar{z}) = M_i(z)/(A_r L^3)$, $\bar{z} = z/L$, $\bar{b} = b/L$, and $\bar{c} = c/L$.

$\overline{\omega}_r = (\bar{c} - \bar{b})[4(\bar{c}^2 + \bar{b}^2) - 3(\bar{c} + \bar{b}) + 4\bar{b}\bar{c}]$, $\overline{w}_g = 2(\bar{b} - \bar{c})[\bar{c}^2 + \bar{b}^2 - (\bar{c} + \bar{b}) + \bar{b}\bar{c}]$. T_i = shear force, and M_i = bending moment. Except for concentrated load *P*-based model, the subscript *i* of 2 and 3 refers to loading and non-loading zone respectively, whereas i = 1 is reserved for non-loading zone from the ground level to depth *b* (see Figure 2)

The maximum bending moment M_{mi} occurs at a depth z_{mi} either in the loading zone, or the non-loading zone. They are given respectively by (Table 2)

Loading zone: $$\overline{M}_{m2} = \frac{(-1 + \overline{\omega}_r)\bar{z}_{m2}^3}{6} + \frac{\overline{w}_g}{2}\bar{z}_{m2}^2 + \frac{\bar{b}^2}{2}\bar{z}_{m2} - \frac{\bar{b}^3}{3} \tag{4a}$$

$$\bar{z}_{m2} = \frac{\overline{w}_g + \sqrt{\overline{w}_g^2 + (1 - \overline{\omega}_r)\bar{b}^2}}{1 - \overline{\omega}_r} \tag{5a}$$

Non-loading zone: $$\overline{M}_{m3} = \frac{\overline{\omega}_r \bar{z}_{m3}^3}{6} + \frac{\overline{w}_g}{2}\bar{z}_{m3}^2 + \frac{1}{2}(\bar{b}^2 - \bar{c}^2)\bar{z}_{m3} - \frac{1}{3}(\bar{b}^3 - \bar{c}^3) \tag{4b}$$

$$\bar{z}_{m3} = \frac{-(\bar{b} + \bar{c})}{4(\bar{b}^2 + \bar{c}^2) - 3(\bar{b} + \bar{c}) + 4\bar{b}\bar{c}} \tag{5b}$$

Note the solutions for $n = 0$ and $n = 1$ are special cases of the power-law solutions. The normalised M_{mi} and z_{mi} are provided for $n = 0$ and $n = 1$ (to facilitate their practical use), but not for other *n*, as the latter can be more readily obtained using the profiles of $M_i(z)$ and $T_i(z)$.

2.2 Parametric Analysis for a Single layer

The new solutions are used next to examine salient features of passive piles in a single layer.

(a) Variations in M_m and z_m

Given a definite loading length of (α-1)b between depths b and c (= αb, see Figure 2), the pile response was obtained with the new solutions, concerning the loading position b. This includes the normalised moment M_m and the depth of the moment, z_m. They are plotted in Figure 4(a) and (b) for α = 1.5, 2.0 and 3, respectively for both constant p and linear p. With increase in the loading depth (to L_s), the normalised depth z_m/L and moment $-M_m/(A_r L^{2+n})$ were obtained for loading zone, and are plotted in Figure 4(a) and (b) as well. The normalised depth z_m/L increases towards the pile tip as the loading length of (α-1)b does (and at a high rate for a high α). This is slightly higher for a linear p profile (n = 1) than that for a uniform p profile (n = 0). The normalised depth z_m and moment M_m were estimated for the non-loading zone, and are depicted together with those for loading zone in Figures 5 and 6, respectively. In particular, the alteration of the 'p' profile from n = 0 to 1 renders the magnitude of the normalised M_m in the non-loading zone reduce by ~16 times, but by only a fraction for that in the loading zone. The loading zone thus dominates the design.

(b) Normalised force and bending moment

The newly established solutions (see Tables 1 through 4) allow the distribution profiles to be obtained, such as the profiles of $T(z)/A_r L^{n+1}$ and $M(z)/A_r L^{n+2}$ for a uniform loading p (n = 0, A_r = p, see Tables 1 and 3), or a linearly increasing p (= $A_r z$, n = 1, Tables 2 and 3) from ground line to depth c, and the profile of $M(z)/PL$ for a concentrated load P (see Table 4), respectively. Figures 7 and 8 provide the normalised shear force $T(z)/pL^{n+1}$, and bending moment $M(z)/pL^{2+n}$ for n = 0 and 1, respectively. It is evident that the normalised force T_m/pL^{n+1} and moment M_m/pL^{n+1} shift with the normalised loading length c/L ($c = L_s$), as is

depicted previously in Figure 6 for the normalised M_m. Figure 9 shows the distribution profiles of normalised bending moment $M(z)/PL$ for a few typical normalised depths of loading by pile embedment (a/L). The maximum moment-force ratio $M(z)/PL$ in Figure 9 is close to the maximum M_m/pL^2 in Figure 8, but the latter (based on distributed p) has a shape close to measured data.

The P-based solution is not recommended for rigid piles (as mentioned earlier). It is included here for comparison, as it has been used successfully for some flexible piles. As for the solutions for a distributed loading p ($= A_r z^n$), a uniform p seems to be critical (compared to other cases) such as the partial loading at depth b to αb (as is seen in anchors), and full loading to depth L_s, which should generally be adopted. The magnitude of increase p should increase proportionally with sliding depth (L_s or αb), as is shown later in an example study.

2.3 Solutions for 2-layered Soil (Passive movement)

Now let's look at a rigid pile embedded in a 2-layered soil, with a moving layer and a stable layer of thickness L_s and λL_s, respectively. Using the p-based model, the impact of soil movement is replaced with a distributed force per unit length p over the sliding depth. Assuming a constant coefficient of subgrade reaction k_s and mk_s in sliding and stable layer, the pressure on the pile in the sliding and stable layer are equal to $k_s w(z)$ and $mk_s w(z)$, respectively. With the p-based model, the solutions for the pile were deduced using force and bending moment equilibriums (not shown herein), which have the following features.

In Equation (1), replacing the A_r with p, the pile deflection at depth z, $w(z)$ is then rewritten as

$$w(z) = (\overline{\omega}_r \overline{z} + \overline{w}_g)\frac{p}{k_s} \qquad (6)$$

where $\overline{\omega}_r$ [= $w'(z)k_sL/p$], and $\overline{w}_g$ (= w_gk_s/p). The shear force $T_i(z)$ and bending moment $M_i(z)$ in the pile at the depths 0 through c (with subscript 1) and the depths c through L (with subscript 2), are expressed as:

$$T_1(z) = [0.5\frac{\overline{\omega}_r}{L}z^2 + \overline{w}_g z - z]p \qquad (z < c) \tag{7a}$$

$$M_1(z) = [\frac{1}{6}\frac{\overline{\omega}_r}{L}z^3 + \frac{1}{2}(\overline{w}_g - 1)z^2]p \qquad (z < c) \tag{8a}$$

$$T_2(z) = \{[\frac{1}{2}(1-m)L_s^2 + \frac{m}{2}z^2]\frac{\overline{\omega}_r}{L} + [(1-m)L_s + mz]\overline{w}_g\}p - pc \qquad (z \geq c) \tag{7b}$$

$$\begin{aligned} M_2(z) = \{&[(\frac{1}{2}L_s^2 z - \frac{1}{3}L_s^3)(1-m) + \frac{m}{6}z^3]\frac{\overline{\omega}_r}{L} \\ &+ [(L_s z - \frac{1}{2}L_s^2)(1-m) + \frac{m}{2}z^2]\overline{w}_g - \frac{c}{2}(2z-c)\}p \end{aligned} \qquad (z \geq c) \tag{8b}$$

where

$$\overline{\omega}_r = \frac{-6cL}{L_s^3}\frac{(2m\lambda + m\lambda^2 + 1)L_s - (m\lambda + 1)c}{1 + 4m\lambda + 6m\lambda^2 + m^2\lambda^4 + 4m\lambda^3} \tag{9}$$

$$\overline{w}_g = \frac{c}{L_s^2}\frac{4(3m\lambda + 3m\lambda^2 + m\lambda^3 + 1)L_s - 3c(2m\lambda + m\lambda^2 + 1)}{1 + 4m\lambda + 6m\lambda^2 + m^2\lambda^4 + 4m\lambda^3} \tag{10}$$

The maximum bending moment M_{mi}, shear force T_{mi} and their respective depths z_{mi} and z_{mti} (subscript i = 1 and 2 for sliding and stable layer, respectively) are as follows.

$$T_{m1} = pz_{mt1}[\frac{1}{2}z_{mt1}\frac{\overline{\omega}_r}{L} + \overline{w}_g - 1] \tag{11}$$

$$M_{m1} = p[\frac{1}{6}\frac{\overline{\omega}_r}{L}z_{m1}^3 + \frac{1}{2}(\overline{w}_g - 1)z_{m1}^2] \tag{12}$$

$$z_{m1} = 2z_{mt1} \tag{13a}$$

$$z_{mt1} = \frac{L_s}{6}\frac{(1+4m\lambda+6m\lambda^2+4m\lambda^3+m^2\lambda^4)L_s^2}{-(1+2m\lambda+m\lambda^2)L_s+c(1+m\lambda)} + \frac{L_s}{6}\frac{-4cL_s(1+3m\lambda+3m\lambda^2+m\lambda^3)+3(1+2m\lambda+m\lambda^2)c^2}{-(1+2m\lambda+m\lambda^2)L_s+c(1+m\lambda)} \quad (13b)$$

$$T_{m2} = p\{[\frac{m}{2}z_{m2}^2+\frac{1-m}{2}L_s^2]\frac{\overline{\omega}_r}{L}+[mz_{m2}+(1-m)L_s]\overline{w}_g - c\} \quad (14)$$

$$M_{m2} = p\{[\frac{m}{6}z_{m2}^3+\frac{1-m}{2}L_s^2z_{m2}+\frac{m-1}{3}L_s^3]\frac{\overline{\omega}_r}{L} + [\frac{m}{2}z_{m2}^2+(1-m)L_sz_{m2}+\frac{m-1}{2}L_s^2]\overline{w}_g - \frac{c}{2}(2z_{m2}-c)\} \quad (15)$$

$$z_{m2} = \frac{L_s}{3}\frac{3c\lambda(m-1)-(1+6m\lambda+3m\lambda^2+m\lambda^3-3\lambda)L_s}{-(1+2m\lambda+m\lambda^2)L_s+c(1+m\lambda)} \quad (16a)$$

$$z_{mt2} = \frac{L_s}{6}\frac{3c(1+2m\lambda+m\lambda^2)-4(1+3m\lambda+3m\lambda^2+m\lambda^3)L_s}{-(1+2m\lambda+m\lambda^2)L_s+c(1+m\lambda)} \quad (16b)$$

Given $\lambda = 0$, and $L_s = L$, the following expressions are deduced

$$\overline{\omega}_r = 6cL(c\text{-}L_s)/L_s^3;\ \overline{w}_g = -c(3c\text{-}4L_s)/L_s^2 \quad (17)$$

$$z_{m2} = L_s^2/3(-c+L_s);\ M_{m2} = \frac{pcm}{54}\frac{(3c-2L_s)^3}{(c-L_s)^2} \quad (18)$$

In comparison with the single layer, these expressions are intended for $b = 0$. Taking $c = L_s$, the normalised rotation $\overline{\omega}_r$ and displacement $\overline{w}_g$ were obtained, along with the normalised depth, z_m/L of maximum bending moment, and depth z_{mt2}/L (in stable layer) of normalised maximum shear force T_m/pL_s. They are plotted in Figure 10 for m = 1, 1.5, 3 and 5 concerning the normalised (a) displacement $\overline{w}_g$; (b) rotation $\overline{\omega}_r$; (c) depth z_{mt}/L for maximum shear force T_m, and depth z_m/L for maximum bending moment M_m; and (d) force T_m/pL_s at various normalised sliding depth L_s.

Finally, the 2-layer solutions for $b = 0$ have been extended to cater for the impact of a uniform and an inverse triangular soil movement profile [12], which provide excellent predications for piles subjected to lateral spreading. The impact of a non-loading zone below ground ($b \neq 0$) is well accounted for by the movement profiles, for which the solutions for 2-layer case is thus not pursued herein. The model and solutions developed here are 'elastic', but they capture the nonlinear response of the piles through increasing the sliding L_s and the associated p [$= p_l L_s/L$, p_l = ultimate force per unit length at pile tip level] [12].

3 COMMENTS

The solutions for rigid piles subjected to a concentrated load P [applied at a depth 'a', see Figure 3(b)] were developed previously [7] for a soil with a uniform k_s. They were re-derived herein to generate these new compact expressions provided in Table 4. The expressions allow the ratios of z_m/L, T_m/P, and $M_m/(PL)$ to be calculated for a set of normalised location a/L ($a = L_s$). The ratios of z_m/L and T_m/P thus obtained are plotted in Figure 10(c) and (d), respectively. The calculated ratios of $M_m/(PL)$ are plotted in Figure 11 concerning positive M_m (rewritten as M_m^+) and negative M_m (i.e. M_m^-), respectively. Note both M_m^+ and M_m^- are plotted as negative to facilitate comparison.

As for a two-layered soil, the normalised moment $M_m/(pL_sL)$ of piles under a total thrust of pL_s ($L_s = c$) was predicted using Equation (12). The normalised values of M_{m2} obtained (with z>c for non-loading zone) are plotted in Figure 11 for the four typical m = 1~5. Both M_m/PL and $M_m/(PL_sL)$ reduce with increase in normalised loading depth L_s/L from a maximum value of 0.148 (at $L_s/L = 0$) to zero (at $L_s/L = \sim 0.8$). Meanwhile, the normalised

depth z_m/L increases from 0.33 to 1.0 [see Figure 10(c)]. The other normalised moment M_m (i.e. M_{m1}) in the loading zone is shown in Figure 11 as well.

The induced ratio of M_m/T_mL was calculated for a concentrated loading P at a normalised loading position a/L = ~ 0.33 (by taking $a = L_s$), and for a two-layered soil with a uniform loading p on the upper layer L_s. The moment M_a at the loading depth a was also calculated. They are all plotted in Figure 12. Importantly, the figure shows a loading at a normalised depth L_s/L of ~0.2 (P-based model) or a sliding over L_s/L of ~0.5 (p-based model) induces a M_m/T_mL ratio of 0.3~0.45. In comparison, the extensive model tests on 'rigid' passive piles in loose to dense sand [5] yield a M_m/T_mL ratio of 0.33 (deep sliding) and 0.39 (shallow sliding) for 50 mm diameter piles; and a ratio of 0.35 and 0.38 for 32 mm diameter piles, regardless of stress level. The current prediction of 0.3~0.45 is thus reasonable against 0.33~ 0.39 from the model tests. In particular, both P-based model and p-based models indicate a higher ratio of 0.38~0.39 for shallow sliding. Under a sliding depth $L_s/L > 0.5$, the M_m may occur at a depth symmetrical about $L_s/L = 0.5$ (see Figure 6) and with the same magnitude.

By taking the length L as the sum of L_s and an effective length (= minimum of pile length L_c in stable layer, and thickness of the stable layer), the ratios of $M_m/(T_mL)$ for eight in-situ test piles [5] were calculated using measured data. They are plotted in Figure 12(a) against the normalised sliding depth L_s/L. The ratios from the flexible piles exhibit similar reduction to the 2-layer prediction with the increasing normalised depth L_s/L. In contrast, the P-based solutions consistently underestimate the ratio of $M_m/(T_mL)$. The former confirms the

success of the p_u-based elastic-plastic solutions [1], while the latter further reveals the inadequacy of the elastic solution based on a thrust P for passive piles.

Viggiani [10] developed useful 'ultimate-state' solutions to design passive piles in 2-layerd clay by assuming a limiting on-pile resistance of p_1 (= k_1c_1) and p_2 (= k_2c_2) in sliding and stable layer, respectively. The solutions are outlined in Table 5 for three reaction modes A, B and C (mode B is normally observed). The modes are classified by a coupled expression involving the impact of the sliding depth ratio λ [= $(L-L_s)/L_s$], and a strength ratio m [= p_2/p_1, and is equal to the modulus ratio]. With the ultimate-state solutions, the normalised maximum shear force T_m/p_1L_s were obtained for a set of L_s/L ratios, and are plotted in Figure 13. Assuming the maximum shearing force occurs at sliding depth L_s, the T_m was also calculated using Equation (7a) by replacing depth z with L_s, and was subsequently normalised by pL_s. The normalised maximum T_m/p_1L_s are compared with the ultimate-state solutions in Figure 13(a). Furthermore, the T_m was calculated using Equation (11) for each L_s (= 0 ~L) and m (= 1.5, 3 and 5); and the normalised T_m is compared with the ultimate-state solutions in Figure 13(b).

In Figure 13, the ultimate-state prediction of the T_m was normalised using a large p_1 of $3.33k_1s_{u1}d$. The front multiplier of 3.33 (= x) was back-estimated by taking $p_1/s_{u1}d = xk_1$ (elastic interaction for passive piles) = 9.14~11.94 (plastic flow for lateral piles) [8]. The empirical value of k_1 was deduced as 2.5~4.0 from measured data [10, 13], thus the x is obtained as 2.3~4.8 (= 9.14~11.94/2.5~4.0). An average '$x \approx 3.33$' is selected to fit to the current solutions. In other words, the current elastic solutions using a fixed $z_{mt} = L_s$ approach the ultimate-state solutions upon using the large ultimate p_l. The measured low p_1 thus implies

a dominant ‘elastic’ response along passive piles, which can be captured using the stipulated distributed p (for the soil movement) rather than the plastic flow around lateral piles, as is evident in model tests on piles in sand [5].

The difference in the normalised T_m between the current and the ultimate solution is evident in Figure 13(b). It reflects the impact of progressive loading of the current solutions, which gradually shifts the depth of maximum shear force z_{mt} to sliding layer (z_{mt1}, Mode A) or to stable layer (z_{mt2} Mode B), rather than $z_{mt} = L_s$. This shift of the depth z_{mt} is evident in instrumented model piles [5], although a fixed depth z_{mt} at sliding interface is seen in field piles (ignoring any transition layer). In model tests for piles in a progressive sliding soil (see Figure 1, and next section) [5], the depth of sliding is not clearly defined. The forcing depth of loading block is generally larger than the depth of maximum shear force z_{mt1} in sliding layer. The depth z_{mt1} and the maximum shear force T_{m1} are thus calculated by using Equations (13b), and (11), respectively; and the maximum bending moment M_{m1} and its z_{m1} calculated by using Equations (13a) and (12), respectively. The normalised maximum shear force T_{m1} and bending moment M_{m1} (for $z_{mt1} \neq L_s$) are plotted in Figure 14 as Mode A.

The thrust should be transferred by the pile to the stable layer. This induces a maximum shear force T_{m2} in the pile at a depth of z_{mt2}, and a maximum bending moment M_{m2} at a depth of z_{m2}. These values were estimated by using Equations (14) through (16). The T_{max2} and M_{m2} estimated are plotted in Figure 14 as Mode B. In particular, the M_{mi} were normalised using the product of pL_sL, (consistent with the normaliser in Figure 11) to avoid large normalised moment at the maximum normalised T_m.

Finally, the normalised maximum bending moment $M_m k_s/pL_s$ and head-displacement $\overline{w}_g$ were obtained and are plotted in Figure 15(a) and (b), respectively. A good comparison with the boundary element solution (BEM) [14] are observed in Figure 15(a) given p/k_s = 0.015 (L/d = 50), 0.18 (25) and 0.35 (10); or in Figure 15(b) by assigning a soil movement w_s as p/k_s. The increase ratio of p/k_s with the decrease in slenderness ratio L/d resembles the trend noted for laterally loaded rigid piles in which $k_s/G_s \approx 10(L/d)^{-0.5}$ [6], although further study in this aspect is recommended.

4 CALCULATION EXAMPLES

4.1 Analysis of A Typical Pile – Arc Profile

Guo and Qin (2010) conducted model tests on passive piles. A pile (L = 0.7 m) was subjected to a triangular (translational) soil movement [see Figure 1(b)] imposed at a distance of 500 mm from the pile and at a sliding depth of 200 mm. The tests provide the measured profiles of bending moment, and shear force along depth (see Figure 16); and the evolution of M_m and w_g with soil movement w_s (see Figure 17). The sand around the piles has a unit weight γ_s' of 16.27 kN/m^3, and a frictional angle of 38^o. Our study shows an average force per unit length p of $0.537\gamma_s' K_p^2 d$, or p = 5 kN/m with d = 32 mm (referred to as d_{32} pile). The shear modulus G_s was 6.52 kPa [14], and the k_s (= $k_o d$) was calculated as 53.2 kPa/m (for the overall sliding) [6].

Assuming a uniform p to a depth of 200 mm (i.e. c/L = 0.29), and k_s = 600 kN/m (justified later), A_r = 72 kN/m, and d = 0.032 m, the profiles for the pile were predicted using the expression in Table 3 (n = 0) and are shown in Figure 16(a) and (b) for bending moment

and shear force for a ground-line displacement w_g of 6.7 mm. The profiles are predicted for the pile with d = 50 mm (or d_{50} pile) as well using the same set of parameters. They agree well with those tests without axial load.

Using the same set of parameters for the constant p case but an A_r of 144 kN/m^2 for linear p case (doubling the A_r value to maintain the average pressure over the sliding depth of 0.29L), the profiles were predicted using the expression in Table 3 (n = 1) for bending moment and shear force. The bending moment profiles (not shown here) resemble those shown in Figure 8(b) for c/L =0.3, featured by two maxima but with magnitudes being much smaller than the constant p predictions [e.g. in Figure 8(a) for c/L =0.3]. The constant p case is more pertinent to the real case, as is identified in our previous study [5].

Assuming m =1.5, and taking the same values of p (= 5.0 kN/m), k_s = 600 kN/m for the d_{32} piles, the prediction using the 2-layer theory is plotted in the figure. As for the d_{50} piles, the p is equal to 7.8 kN/m (= 5*50/32), k_s = 938 kN/m (= 600*50/32) using the parameters for d_{32} piles and considering the proportional increase in k_s and p with the diameter. The prediction is plotted in Figure 16 as well.

The predictions using a single layer (m =1), or 2-layer (m =1.5) are close to measured data, but with a high value k_s = 600 kN/m than deduced previously. The latter is attributed to the use of a fixed loading depth (L_s). The actual sliding depth at the pile location is smaller than L_s during the progressive soil movement. Using a real k_s of 60 kPa (mentioned earlier), the maximum bending moment and pile-head displacement were predicted using the 2-layer theory of Equations (15) and (10), respectively and m = 7 for piles without vertical load P_t on pile head (or m =11 with a load P_t), by gradually increasing the sliding depth L_s and the p [=

$12.5L_s/L$ (kN/m)]. It shows an excellent match with the measured nonlinear response (see Figure 17), and the ultimate moment observed using deep sliding depth (shown elsewhere). This set of m and k_s also predict well the variation of bending moment, and pile deflection with depth (see Figure 18), but overestimate the maximum shear force and on-pile force per unit.

In the same manner, the response for a few piles tested in moving soil with a uniform, an inverse triangular, or an arc soil movement profile was predicted using the 2-layer model. The maximum shear force and on-pile force per unit length are constantly overestimated against measured data for each movement profile, as with those presented in Fig. 16. The overestimation is attributed to the neglecting of the transition in the modulus from k_s to mk_s, (dragging impact), which is currently being examined.

CONCLUSIONS

This paper proposes new p-based pile-soil interaction models and develops their associated solutions to capture response of rigid piles subjected to soil movement. The impact of soil movement was encapsulated into a power-law distributed loading p over a sliding depth, and load transfer model was adopted for the piles-soil interaction. Regarding a single layer, the solutions are provided as function of loading depth ($b \sim \alpha b$, c, or L_s), and the p (via the gradient A_r). As for a 2-layer profile, the solutions are developed for a uniform p to a sliding depth L_s, which is underlined by subgrade modulus k_s, mk_s for sliding and stable layer, respectively.

Given the input values of m, k_s and p_l, the nonlinear response of passive pile can be readily obtained using the 2-layer solution by gradually increasing L_s [thus p ($= p_l L_s/L$)]. The

solutions reveal the impact of sliding depth and relative strength between sliding and stable layer on limiting force prior to ultimate state; and the one-third limiting pressure (of the active piles) induced on passive piles by elastic interaction. The current models employing distributed pressure to capture impact of moving soil are more pertinent to passive piles (rather than plastic soil flow or concentrated load at sliding depth). The fixing of maximum shear force at L_s or not offer significantly different values of T_m. An example calculation against instrumented model piles is provided, which demonstrates the accuracy of the current solutions for design slope stabilising piles.

The model of pile and soil displacement and values of m and p are further confirmed elsewhere in light of more measured data [12]. Given an inclined sliding and complex geometrical layers, a modulus k_s and ratio m should be determined for the entire sliding layer, and stable layer, which allow the p-based model (for piles in one or two horizontal soil layers) to be applied. In particular, the 2-layer model and solutions offer excellent predictions to measured response of pertinent piles subjected to lateral spreading [12].

NOTATION

The following symbols are used in the paper:

A_r = coefficient for the force per unit length;

a, b, c = loading depths

d = diameter of an equivalent solid cylinder pile;

G_s = average soil shear modulus over the pile length, L;

k_i = coefficient for limiting resistance for upper layer (i = 1) and lower layer (i = 2);

k_s = a uniform coefficient of subgrade reaction;

L = embedded pile length;

L_s = thickness of a upper moving soil layer;

$\overline{M}_i(\bar{z})$ = $M_i(z)/(A_r L^3)$, normalised bending moment at depth z, M_i = bending moment;

M_m, M_o, $M(\bar{x})$ = maximum bending moment within a pile, and that occurs at the mudline level; the moment at the normalised depth $\bar{x}$;

$\overline{M}_m$ = $M_m \lambda^{2+n}/A_L$, normalised M_m;

m = ratio of the lower layer p over that of the upper layer;

n = power for the ultimate force per unit length p;

P = equivalent concentrated load at sliding depth;

P_t = vertical load on passive piles during model tests;

p_1, p_2 = ultimate force per unit length over sliding and stable layer, respectively;

p_u = limiting force per unit length;

$p(z)$ = net force per unit length at the depth z;

$s_u(\tilde{s}_u)$ = undrained shear strength of soil (Average s_u over a maximum slip depth anticipated);

T_m = maximum shear force induced in a passive pile;

$\overline{T}_i(\bar{z})$ = $T_i(z)/(A_r L^2)$ normalised shear force at depth z, T_i = shear force;

w_g = pile deflection at ground level;

w_s = soil movement in model pile tests;

$\overline{w}_g$ = $w_g k_s/(A_r L^n)$, normalised displacement;

$w(z), w'(z)$ = deflection and rotation at the depth z;

z, $\bar{z}$ = depth and the normalised depth z/L, respectively;

$z_{m,}$ z_{mi} = depth of maximum bending moment;

z_{mt} = depth for maximum shear force T_m;

α = parameter (>1.0), αb is loading depth [see Figure 4(a)];

λ = ratio of thickness of lower stable layer over sliding layer;

$\gamma_s(\gamma_s')$ = unit weight of the overburden soil (effective γ_s);

ω_r = rotation angle of pile at ground-level

$\overline{\omega}_r$ = $w'(z)k_s/(A_rL^{n-1})$, normalised rotation;

ν_s = Poisson's ratio of soil, taken as 0.25 for sand, otherwise 0.4;

Bar '-' for normalised parameters and variables.

Appendix A Solutions for two-layered *p* profile

In this appendix, derivation of the elastic solutions for the pile in two-layered in the paper is elaborated. All of the symbols used are of identical meanings to those defined earlier.

A.1 Pile Response at Pre-tip Yield State

The force per unit length p of $p_1 = k_s w(z)$ *and* $p_2 = mk_s w(z)$, allows the horizontal force equilibrium of the rigid pile (see Figure $3a_1$) to be written as

[A1] $$\int_o^{L_s} (\overline{\omega}_r s + \overline{w}_g)\, p ds + \int_{L_s}^{L} (\overline{\omega}_r s + \overline{w}_g)\, pm ds = 0$$

The integration is made with respect to 's'. The moment equilibrium about the pile-head offers

[A2] $$\int_o^{L_s} (\overline{\omega}_r s + \overline{w}_g)\, p(z-s) ds + \int_{L_s}^{L} (\overline{\omega}_r s + \overline{w}_g)\, pm(z-s) ds = 0$$

Equations [A1] and [A2] allow the $\overline{\omega}_r$ and $\overline{w}_g$ to be determined as Equations (9) and (10).

The expressions for the $T(z)$ and $M(z)$ are deduced. By $T_i'(z) = 0$, the depth of maximum shear force T_{mi}, z_{mti} is determined; whereas with $M_1'(z) = 0$, the depth of the maximum shear force M_{mi}, z_{mi} is gained.

Appendix B References

1. Guo, W.D., *P_u-based solutions for slope stabilizing piles.* International Journal of Geomechanics, 2013; **13**(3): 292-310.
2. Abdoun, T., R. Dobry, T.D. O'Rourke, and S.H. Goh, *Pile response to lateral spreads: Centrifuge modeling.* J. Geotech. and Geoenviron. Engrg, ASCE, 2003; **129**(10): 869-878.
3. Boulanger, R.W., B.L. Kutter, S.J. Brandenberg, P. Singh, and D. Chang, *Pile foundations in liquefied and laterally spreading ground during earthquakes: Centrifuge experiments and analyses*, in *Rep. No. UCD/CGM-03/01, Center for Geotechnical Modeling, Univ. of California, Davis*. 2003: California, USA.
4. Cubrinovskia, M., T. Kokushob, and K. Ishihara, *Interpretation from large-scale shake table tests on piles undergoing lateral spreading in liquefied soils.* Soil Dynamics and Earthquake Engineering, 2006; **26**: 275-286.
5. Guo, W.D. and H.Y. Qin, *Thrust and bending moment of rigid piles subjected to moving soil.* Canadian Geotechnical Journal, 2010; **47**(2): 180-196.
6. Guo, W.D., *Theory and practice of pile foundations*. 2012, Boca Raton, London, New York: CRC press, Taylor & Francis Group.
7. Scott, R.F., *Foundation analysis*. 1981, N. J.: Prentice Hall, Englewood Cliffs.
8. Randolph, M.F. and G.T. Houlsby, *The limiting pressure on a circular pile loaded laterally in cohesive soil.* Geotechnique, 1984; **34**(4): 613-623.
9. Guo, W.D. and F.H. Lee, *Load transfer approach for laterally loaded piles.* International Journal for Numerical and Analytical Methods in Geomechanics, 2001; **25**(11): 1101-1129.
10. Viggiani, C. *Ultimate lateral load on piles used to stabilise landslide*. in *Proc. 10th Int. Conf. Soil Mech. and Found. Engrg.* 1981; Stockholm, Sweden.
11. Guo, W.D., *Laterally piles in cohesionless soil.* Canadian Geotechnical Journal, 2008; **45(5)**: 676-697.
12. Guo, W.D., *Modelling passive piles from sliding soil to lateral spreading.* Computers and Geotechnics, 2014: to be submitted.
13. Poulos, H.G., *Design of reinforcing piles to increase slope stability.* Canadian Geotechnical Journal, 1995; **32**(5): 808-818.
14. Chen, L.T. and H.G. Poulos, *Piles subjected to lateral soil movements.* Journal of Geotechnical and Geoenvironmental Engineering, American Society of Civil Engineers, 1997; **123**(9): 802-811.
15. Qin, H.Y., *Response of pile foundations due to lateral force and soil movements*, in *School of Engineering*. 2010; Griffith University: Gold Coast.

Table 1 M_m and z_m for piles with a constant p over depths b through c

Depth	Expressions	
$b \sim c$	$\overline{M}_{m2} = \frac{\overline{\omega}_r \bar{z}_{m2}^3}{6} + \frac{(\overline{w}_g - 1)}{2}\bar{z}_{m2}^2 + \frac{\overline{b}}{2}\bar{z}_{m2} - \frac{\overline{b}^2}{2}$	(Loading zone)
	$\bar{z}_{m2} = -\frac{\overline{w}_g - 1 + \sqrt{(\overline{w}_g - 1)^2 - 2\overline{b}\,\overline{\omega}_r}}{\overline{\omega}_r}$	(Loading zone)
$c \sim$ L	$\overline{M}_{m3} = \frac{\overline{\omega}_r \bar{z}_{m3}^3}{6} + \frac{\overline{w}_g}{2}\bar{z}_{m3}^2 + \frac{\overline{b} - \overline{c}}{2}\bar{z}_{m3} + \frac{\overline{c}^2 - \overline{b}^2}{2}$	(Non-loading zone)
	$\bar{z}_{m3} = -\frac{\overline{w}_g - \sqrt{\overline{w}_g^2 + 2(\overline{c} - \overline{b})\overline{\omega}_r}}{\overline{\omega}_r}$	(Non-loading zone)
Note	*Single layer, constant k_s and constant p (over $z = b \sim c$).* $\overline{M}_{mi} = M_{mi}/(A_r L^2)$, the values of $\overline{\omega}_r$ [$= w'(z)k_s/(A_r L^{n-1})$], and $\overline{w}_g$ [$= w_g k_s/(A_r L^n)$] are determined using Table 3 with n = 0.	

Table 2 M_m and z_m for piles with a linear p over depths b through c

Depth	Expressions
$b \sim c$	$\overline{M}_{m2} = \frac{(-1+\overline{\omega}_r)\overline{z}_{m2}^3}{6} + \frac{\overline{w}_g}{2}\overline{z}_{m2}^2 + (\frac{\overline{b}^2}{2}\overline{z}_{m2} - \frac{\overline{b}^3}{3})$ (Loading zone)
	$\overline{z}_{m2} = \frac{\overline{w}_g + \sqrt{\overline{w}_g{}^2 + \overline{b}^2(1-\overline{\omega}_r)}}{1-\overline{\omega}_r}$ (Loading zone)
$c \sim$ L	$\overline{M}_{m3} = \frac{\overline{\omega}_r \overline{z}_{m3}^3}{6} + \frac{\overline{w}_g}{2}\overline{z}_{m3}^2 + \frac{\overline{b}^2 - \overline{c}^2}{2}\overline{z}_{m3} + \frac{\overline{c}^3 - \overline{b}^3}{3}$ (Non-loading zone)
	$\overline{z}_{m2} = \frac{-\overline{w}_g + \sqrt{\overline{w}_g{}^2 - (\overline{b}^2 - \overline{c}^2)(1-\overline{\omega}_r)}}{\overline{\omega}_r}$ (Non-loading zone)
Note	*Single layer, constant k_s and linear p (over $z = b \sim c$).* $\overline{M}_{mi} = M_{mi}/(A_r L^3)$, the values of $\overline{\omega}_r$ [$= w'(z)k_s/(A_r L^{n-1})$], and $\overline{w}_g$ [$= w_g k_s/(A_r L^n)$] are determined using Table 3 with n = 1.

Table 3 Solutions for piles with $p = A_r z^n$ (Passive movement)

Depth $\bar{z}$	Expressions
$0 \sim L$	$w(\bar{z}) = (\bar{\omega}_r \bar{z} + \bar{w}_g)\dfrac{A_r L^n}{k_s}$ $\bar{\omega}_r = \dfrac{-6[2\bar{b}(n+1)-2-n]\bar{b}^{n+1} + 6[2\bar{c}(1+n)-2-n]\bar{c}^{n+1}}{(n+1)(2+n)}$ $\bar{w}_g = \dfrac{[6\bar{b}(n+1)-4(n+2)]\bar{b}^{n+1} - [6\bar{c}(n+1)-4(n+2)]\bar{c}^{n+1}}{(n+1)(2+n)}$
$0 \sim \bar{b}$	$\bar{T}_1(\bar{z}) = \dfrac{1}{2}\bar{\omega}_r \bar{z}^2 + \bar{w}_g \bar{z}$, $\bar{M}_1(\bar{z}) = \dfrac{\omega_r \bar{z}^{2+n}}{6} + \dfrac{\bar{w}_g}{2}\bar{z}^2$
$\bar{b} \sim \bar{c}$	$\bar{T}_2(\bar{z}) = \dfrac{1}{2}\bar{\omega}_r \bar{z}^2 + \bar{w}_g \bar{z} + \dfrac{1}{1+n}(\bar{b}^{n+1} - \bar{z}^{n+1})$ $\bar{M}_2(\bar{z}) = \dfrac{\bar{\omega}_r \bar{z}^3}{6} + \dfrac{\bar{w}_g}{2}\bar{z}^2 + [\dfrac{\bar{b}^{n+1}}{n+1}\bar{z} - \dfrac{(1+n)\bar{b}^{n+2} + \bar{z}^{2+n}}{(n+2)(n+1)}]$
$\bar{c} \sim 1$	$\bar{T}_3(\bar{z}) = \dfrac{1}{2}\bar{\omega}_r \bar{z}^2 + \bar{w}_g \bar{z} + \dfrac{1}{1+n}(\bar{b}^{n+1} - \bar{c}^{n+1})$ $\bar{M}_3(\bar{z}) = \dfrac{\bar{\omega}_r}{6}\bar{z}^3 + \dfrac{\bar{w}_g}{2}\bar{z}^2 + [\dfrac{\bar{b}^{n+1} - \bar{c}^{n+1}}{n+1}\bar{z} + \dfrac{\bar{c}^{2+n} - \bar{b}^{2+n}}{n+2}]$
Note	*Single layer, constant k_s and $p = A_r z^n$ ($z = 0 \sim c$)* $\bar{T}_i(\bar{z}) = T_i(z)/(A_r L^{1+n})$, $\bar{M}_i(\bar{z}) = M_i(z)/(A_r L^{2+n})$, $\bar{\omega}_r = w'(z)k_s/(A_r L^{n-1})$, $\bar{w}_g = w_g k_s/(A_r L^n)$

Table 4 Solutions for piles under a concentrated load (Passive movement)

Depth $\bar{z}$	Expressions
0~ $\bar{a}$	$\overline{T}_1(\bar{z}) = [3(2\bar{a}-1)\bar{z} + 2(-3\bar{a}+2)]\bar{z}$ $\overline{M}_1(\bar{z}) = [(2\bar{a}-1)\bar{z} + (-3\bar{a}+2)]\bar{z}^2$
$\bar{a}$ ~1	$\overline{T}_2(\bar{z}) = [3(2\bar{a}-1)\bar{z} + 2(-3\bar{a}+2)]\bar{z} - 1$ $\overline{M}_2(\bar{z}) = [(2\bar{a}-1)\bar{z} + \bar{a}](\bar{z}-1)^2$
0~1	$w(\bar{z}) = [3(2\bar{a}-1)\bar{z} + (-3\bar{a}+2)]\frac{2P}{k_s L}$
$\bar{a} \neq 0.5$	$\overline{T}_{m1} = \frac{-(3\bar{a}-2)^2}{3(2\bar{a}-1)}$, $\overline{T}_{m2} = \frac{-(3\bar{a}-1)^2}{3(2\bar{a}-1)}$, $\bar{z}_{m1} = \frac{2(3\bar{a}-2)}{3(2\bar{a}-1)}$, $\overline{M}_{m1} = \frac{-4(3\bar{a}-2)^3}{27(2\bar{a}-1)^2}$, $\overline{M}_{m2} = \frac{9\bar{a}-4}{27(2\bar{a}-1)^2} + \bar{a}$, $\bar{z}_{m2} = \frac{-1}{3(2\bar{a}-1)}$ $\overline{T}_m = 0.5$, $\overline{M}_{m1} = \overline{M}_{m2} = 1/8$
Note	• *Single layer, constant k_s, with P at depth a* • $\overline{T}_i(\bar{z}) = T_i(z)/P$, $\overline{M}_i(\bar{z}) = M_i(z)/(PL)$,

Table 5 'Ultimate state' solutions (Viggaini, 1981) for piles in 2-layered soil

Mode	Expressions
A	With $\lambda < \lambda_A = (\sqrt{\frac{2(1+m)}{m}} - 1)/(2+m)$ $\overline{T}_A = T_A/(k_1 c_1 d L_s) = m\lambda$, $\overline{M}_{2A} = M_{2A}/(k_1 c_1 d L_s^2) = 0.5 m\lambda^2$
B	With $\lambda > \lambda_A = (\sqrt{\frac{2(1+m)}{m}} - 1)/(2+m)$ $\overline{T}_B = T_B/(k_1 c_1 d L_s) = \sqrt{[\frac{(1+\lambda)m}{1+m}]^2 + [\frac{(m\lambda^2+1)m}{1+m}]} - \frac{(1+\lambda)m}{1+m}$, $\overline{M}_{1B} = M_{1B}/(k_1 c_1 d L_s^2) = (1-\overline{T}_B)^2/4$, $\overline{M}_{2B} = M_{2B}/(k_1 c_1 d L_s^2) = \frac{m}{4}(\lambda - \frac{\overline{T}_B}{m})^2$
C	With $\lambda > \lambda_c = \frac{1+\sqrt{2(1+m)}}{m}$ $\overline{T}_C = T_C/(k_1 c_1 d L_s) = 1$, $\overline{M}_{1c} = M_{1c}/(k_1 c_1 d L_s^2) = 0.5$
Note	*Two layered,* $\lambda = (L - L_s)/L_s$, $m = k_2 c_2/(k_1 c_1)$

Figure Captions

Figure 1 Rigid piles tested under either of the indicated soil movement profile: (a) Uniform movement (b) Inverse triangular movement (c) Arc movement

Figure 2 p-based models of passive piles using typical profiles of p (single layer): (a) Constant $p = A_r$ with (a_1) pile-soil system, (a_2) p applied and p(z) induced; (b) Linear $p = A_r z$ with (b_1) pile-soil system, (b_2) p applied and p(z) induced; and (c) Parabolic $p = A_r z^n$ with (c_1) pile-soil system, (c_2) p applied and p(z) induced

Figure 3 p-based models of passive piles using uniform p and mp or or P-based model using concentrated load P: (a) 2-layered constant p with (a_1) pile-soil system, (a_2) p applied and p(z) induced; and (b) Concentrated load P with (b_1) pile-soil system, (b_2) P applied and p(z) induced

Figure 4 Response to normalised loading length (single layer): (a) z_{m2}/L, and (b) $M_{m2}/(A_r L^{2+n})$

Figure 5 Normalised depth z_{mi}/L versus normalized loading length (single layer)

Figure 6 Variations of $M_{mi}/(A_r L^{2+n})$ with normalized loading length (single layer)

Figure 7 Normalized shear force with depth (p over depths 0 through c)

Figure 8 Normalized bending moment with depth (p over depths 0 through c)

Figure 9 Distribution of $M(z)/PL$ (Concentrated load P at depth a) with normalized depth

Figure 10 Normalized critical pile response versus L_s/L relationship: (a) Normalized $\overline{w}_g$ for w_g; (b) Normalized $\overline{\omega}_r$ for w_g; (c) z_{mt2}/L and z_{m2}/L, and (d) $T_{m2}/(pL_s)$ or T_{m2}/P

Figure 11 Normalized maximum bending moment of $M_m/(PL)$ or $M_m/(pL_sL)$ versus L_s/L

Figure 12 $M_m/(T_mL)$ versus normalized depth L_s/L

Figure 13 $T_m/(pL_s)$ versus normalized length (p force per unit length): (a) T_m fixed at depth L_s; (b) T_m not fixed at depth L_s

Figure 14 $M_m/(pLL_s)$ versus normalized loading length L_s/L

Figure 15 Comparison between current solution and BEM results [14]: (a) Normalized bending moment; (b) Normalized deflection

Figure 16 Predicted versus measured [5] response profiles of 2 tests (final sliding depth = 0.29L, and w/o axial load): (a) Bending moment; (b) Shear force

Figure 17 Comparison between 2-layer theory and the measured [15] curves of $w_g \sim M_m$ for passive piles with vertical loading

Figure 18 Response of pile duringTS32-294 (Prediction using m =11, L_s= 190 mm)

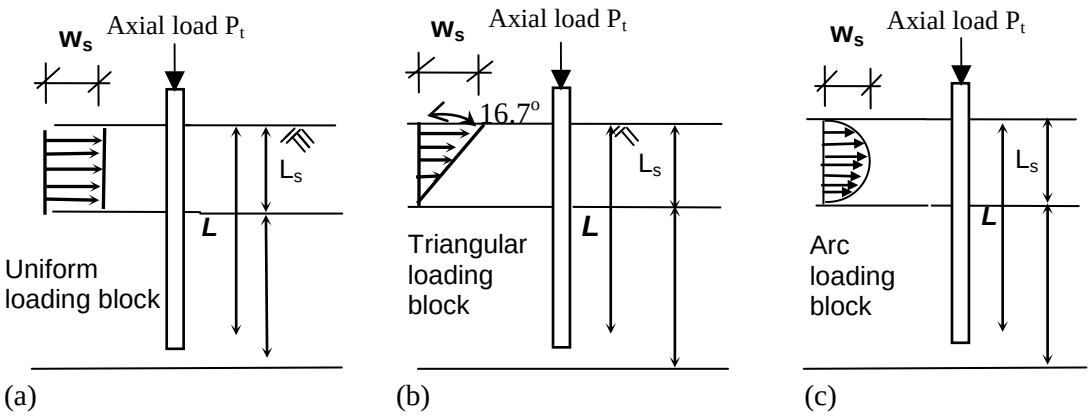

Figure 1 Rigid piles tested under either of the indicated soil movement profile:
(a) Uniform movement (b) Inverse triangular movement (c) Arc movement

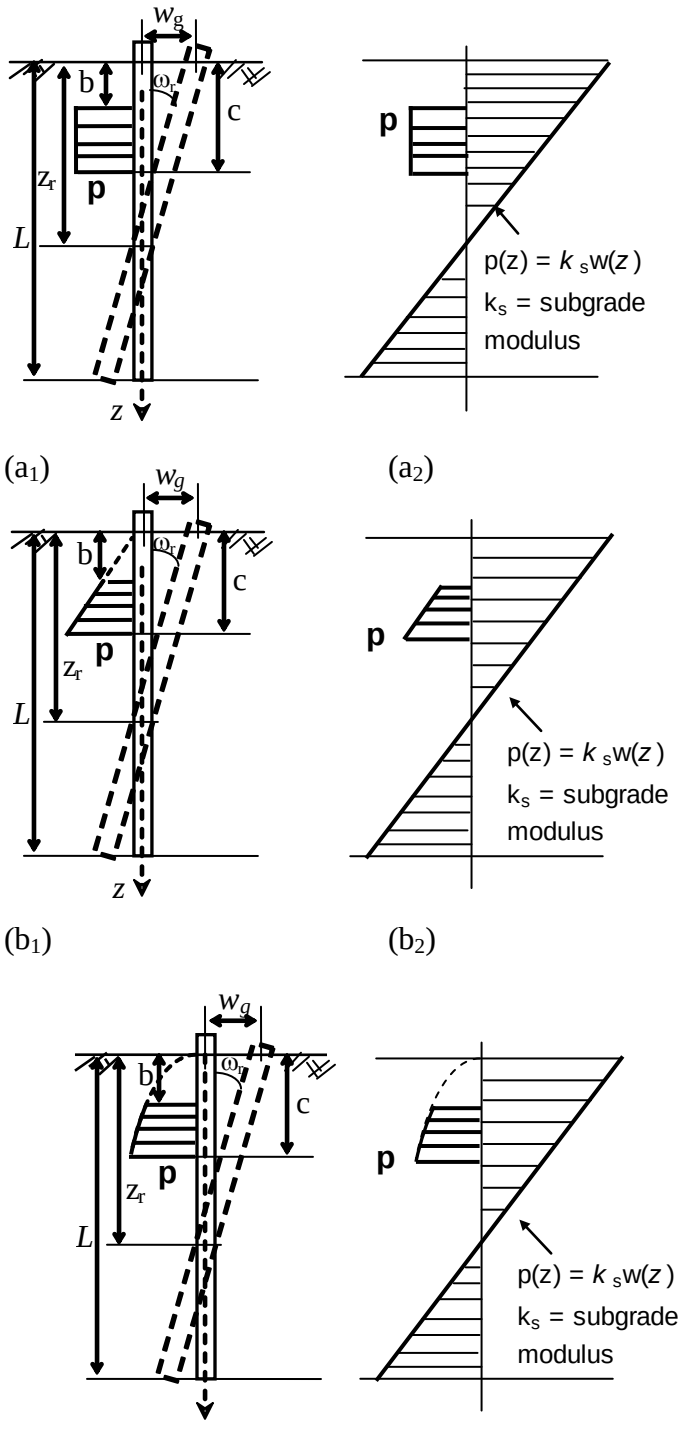

Figure 2 p-based models of passive piles using typical profiles of p (single layer): (a) Constant $p = A_r$ with (a_1) pile-soil system, (a_2) p applied and p(z) induced; (b) Linear $p = A_r z$ with (b_1) pile-soil system, (b_2) p applied and p(z) induced; and (c) Parabolic $p = A_r z^n$ with (c_1) pile-soil system, (c_2) p applied and p(z) induced

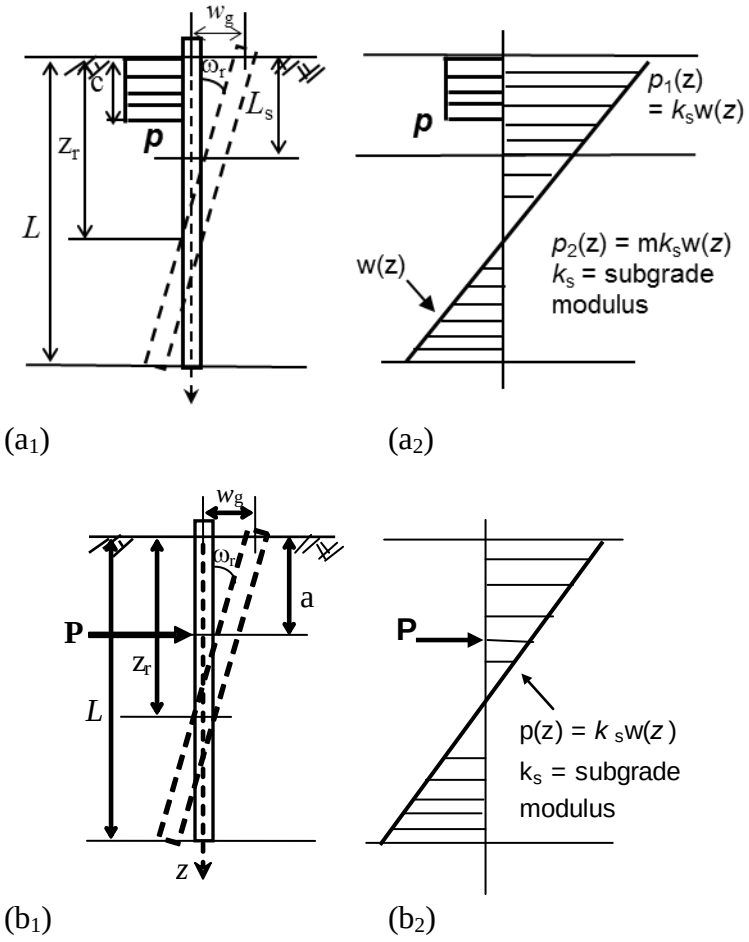

Figure 3 p-based models of passive piles using uniform *p* and *mp* or *P*-based model using concentrated load *P*: (a) 2-layered constant *p* with (a_1) pile-soil system, (a_2) *p* applied and *p*(z) induced; and (b) Concentrated load *P* with (b_1) pile-soil system, (b_2) *P* applied and *p*(z) induced

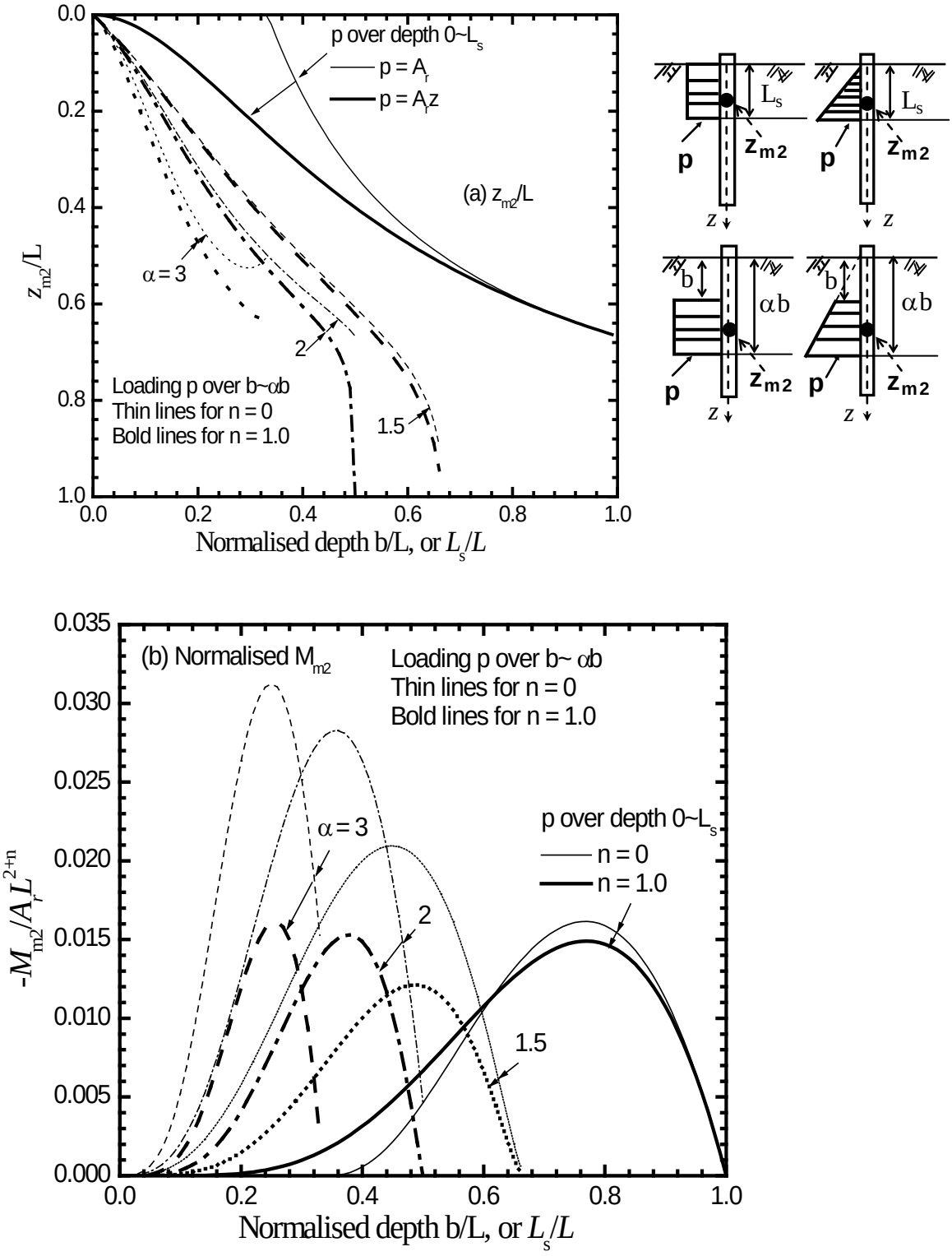

Figure 4 Response to normalized loading length (single layer): (a) z_{m2}/L, and (b) $M_{m2}/(A_r L^{2+n})$

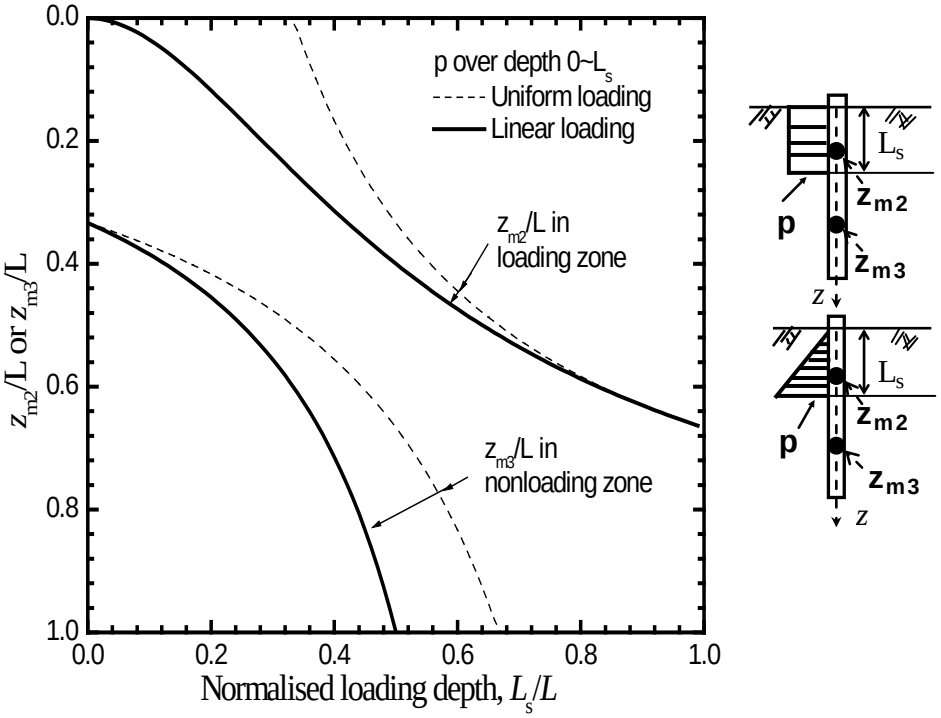

Figure 5 Normalised depth z_{mi}/L versus normalized loading length (single layer)

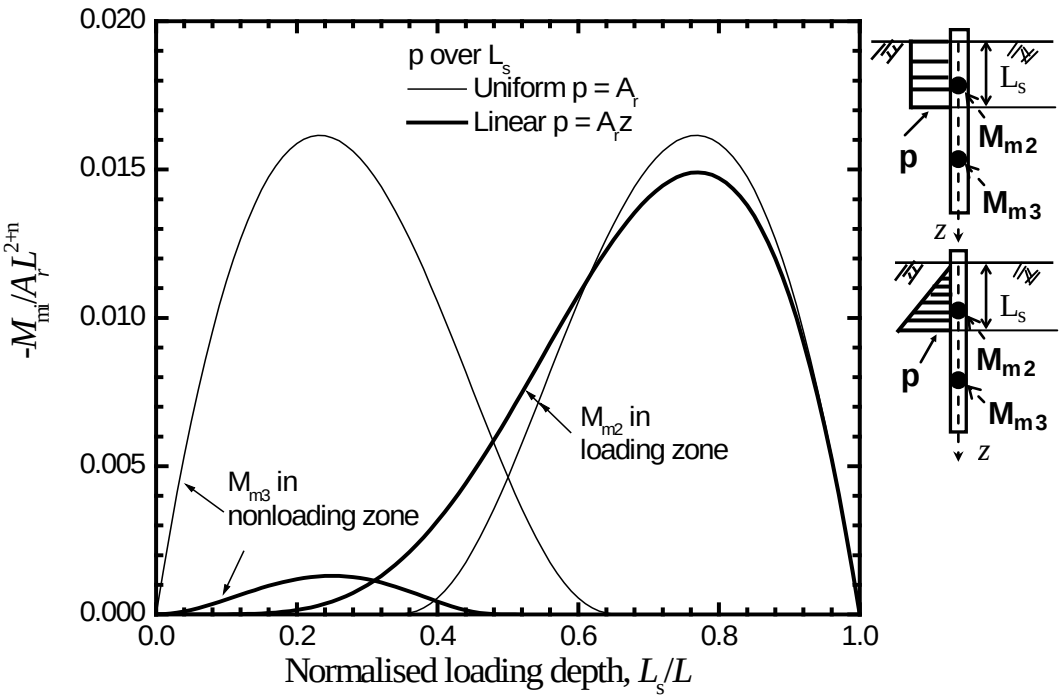

Figure 6 Variations of $M_{mi}/(A_r L^{2+n})$ with normalized loading length (single layer)

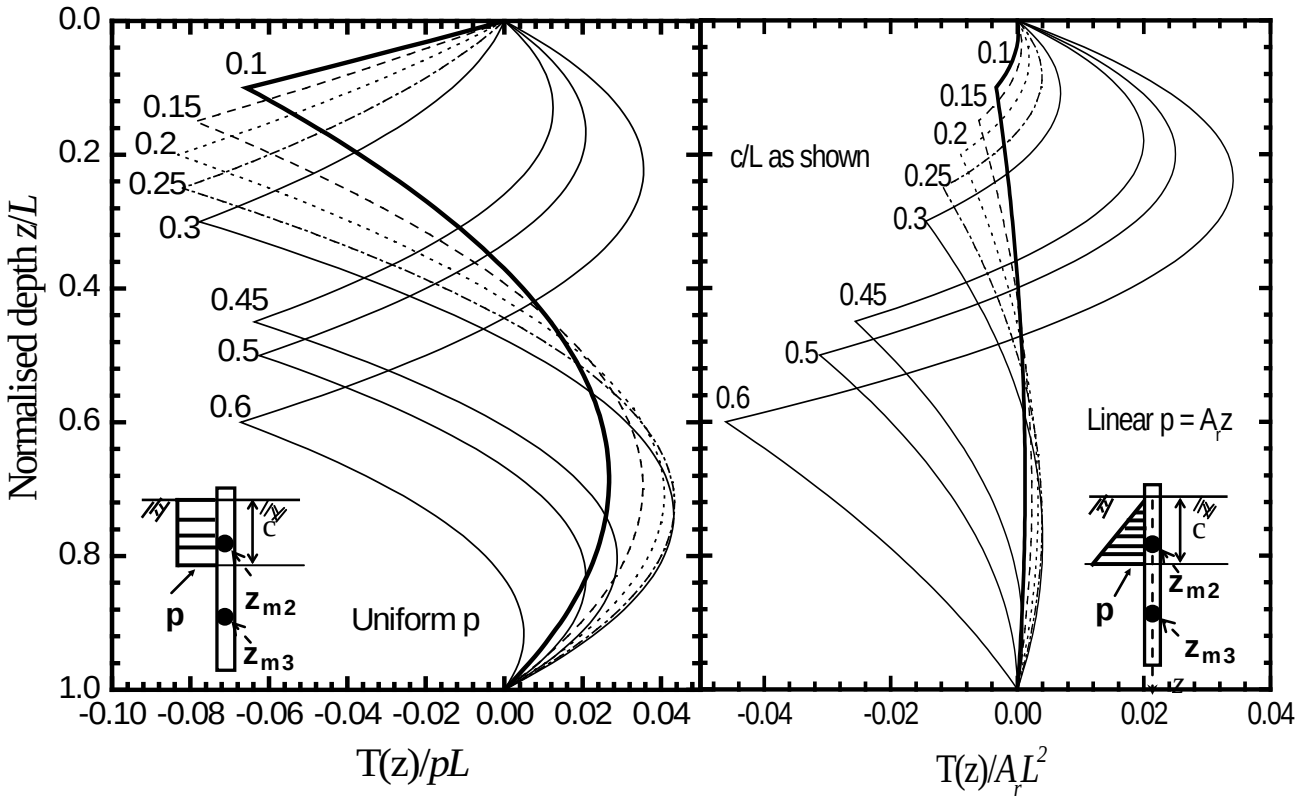

Figure 7 Normalized shear force with depth (*p* over depths 0 through *c*)

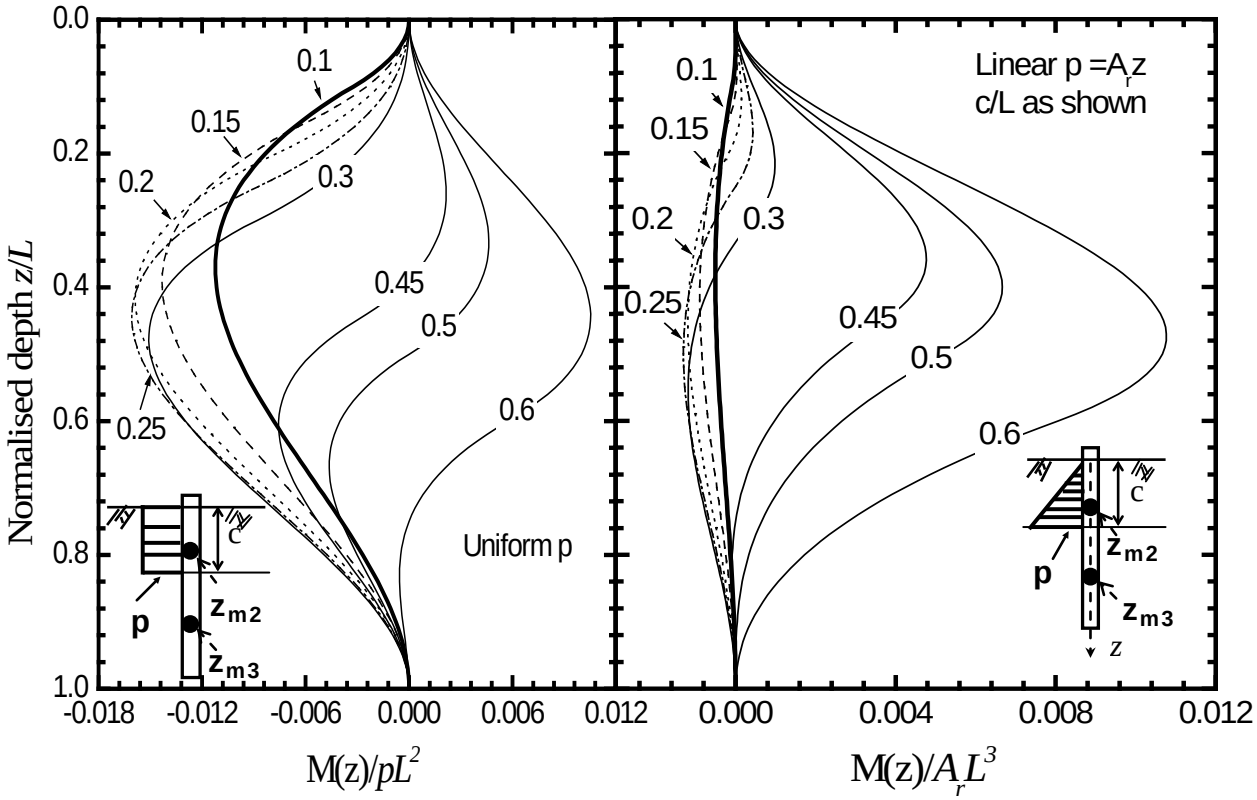

Figure 8 Normalized bending moment with depth (*p* over depths 0 through *c*)

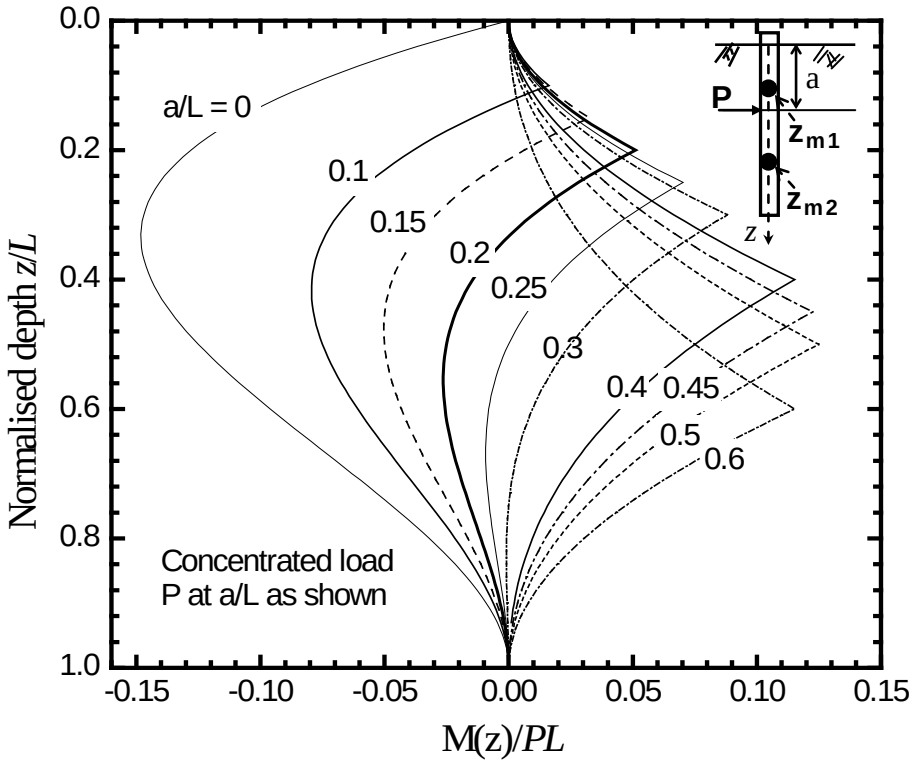

Figure 9 Distribution of $M(z)/PL$ (Concentrated load P at depth 'a') with normalized depth

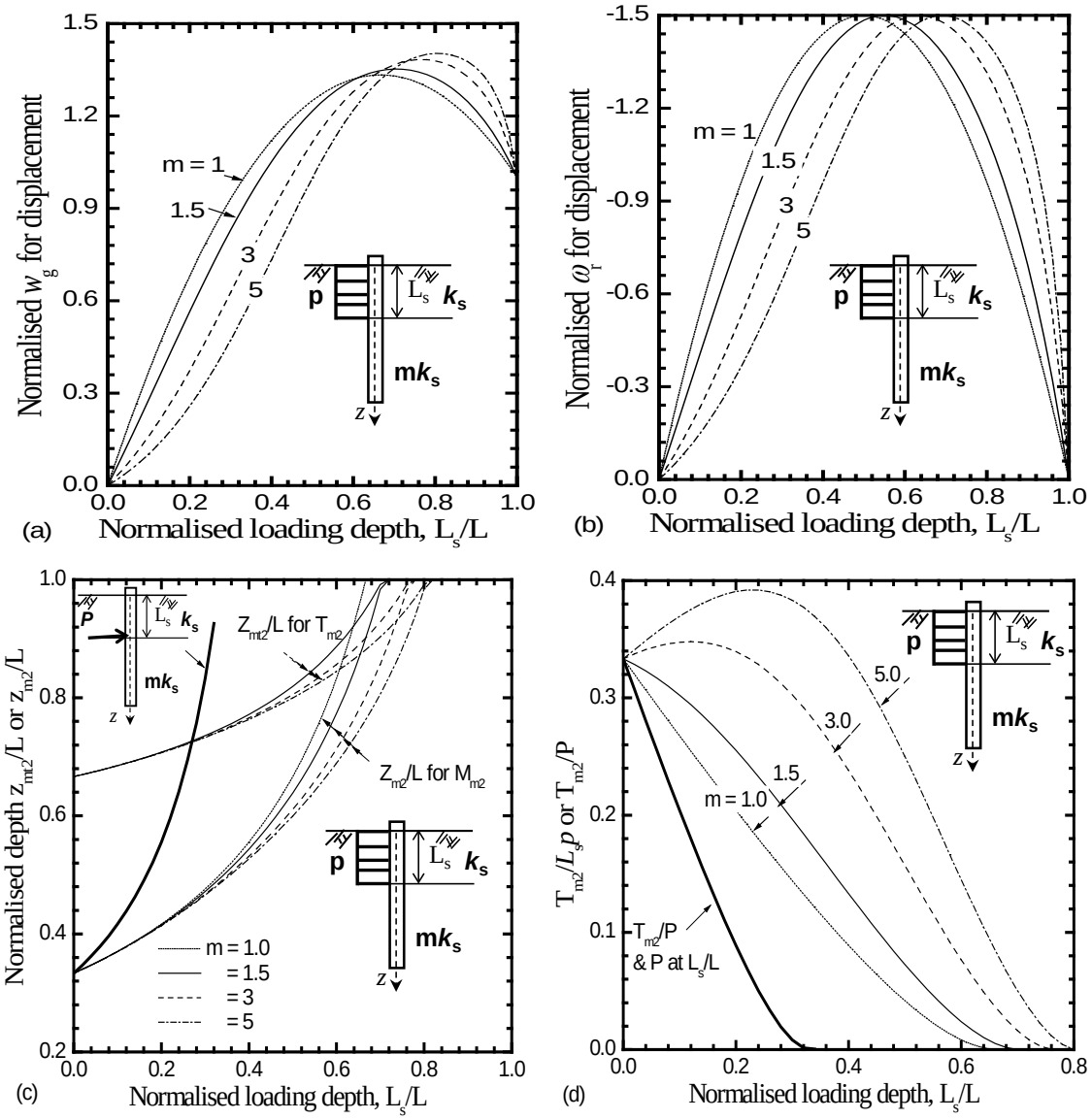

Figure 10 Normalized critical pile response versus L_s/L relationship: (a) Normalized $\overline{w}_g$ for w_g; (b) Normalized $\overline{\omega}_r$ for w_g; (c) z_{mt2}/L and z_{m2}/L, and (d) $T_{m2}/(pL_s)$ or T_{m2}/P

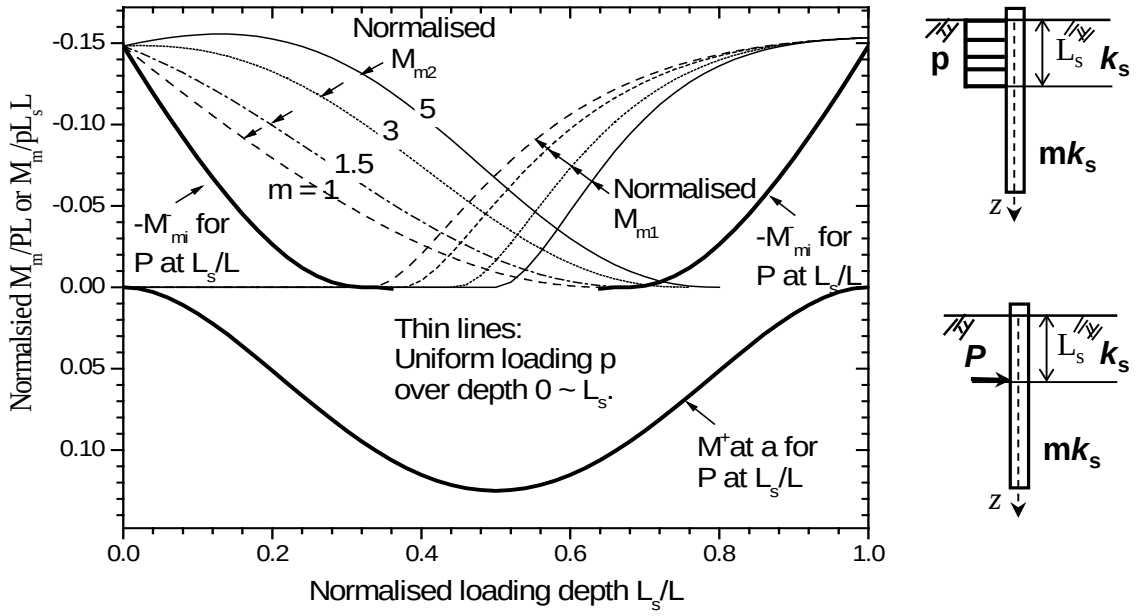

Figure 11 Normalized maximum bending moment of $M_m/(PL)$ or $M_m/(pL_sL)$ versus L_s/L

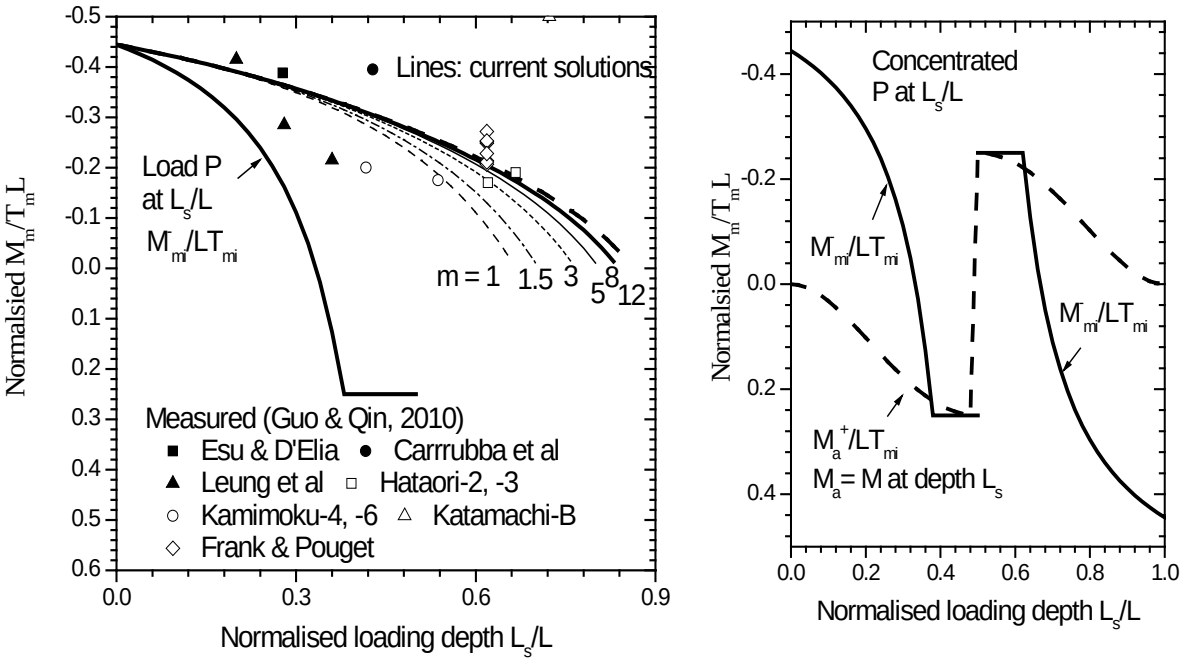

Figure 12 $M_m/(T_mL)$ versus normalized depth L_s/L

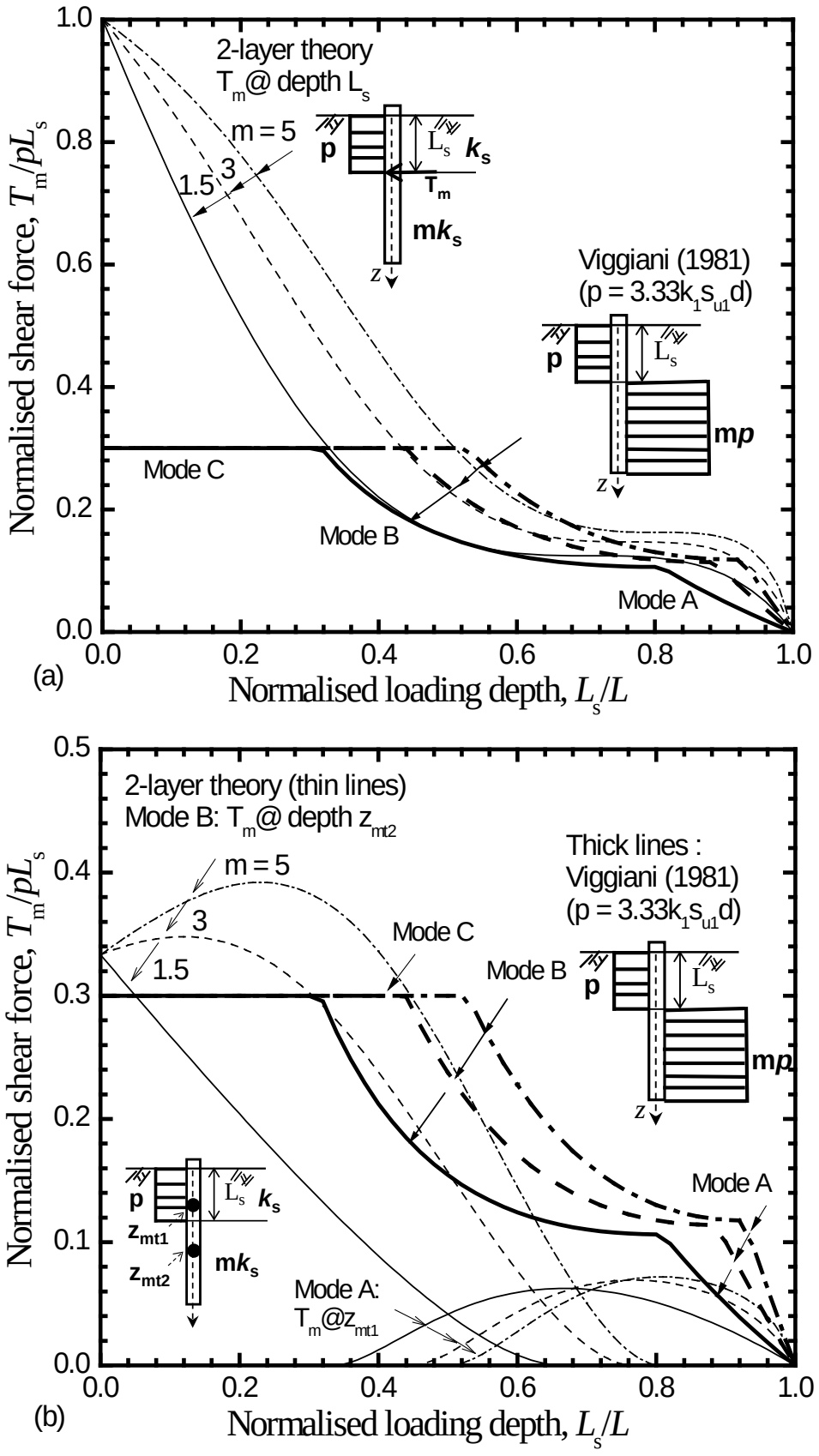

Figure 13 $T_m/(pL_s)$ versus normalized length (p force per unit length): (a) T_m fixed at depth L_s; (b) T_m not fixed at depth L_s

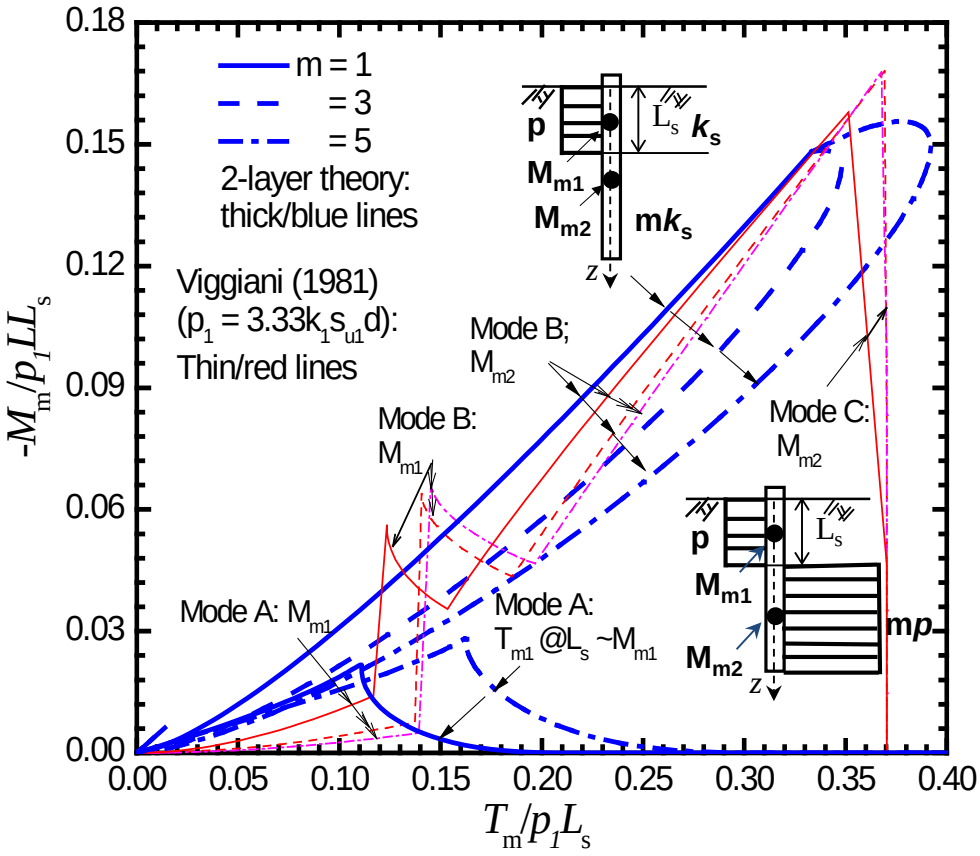

Figure 14 $M_m/(pLL_s)$ versus normalized shear force T_m/p_1L_s

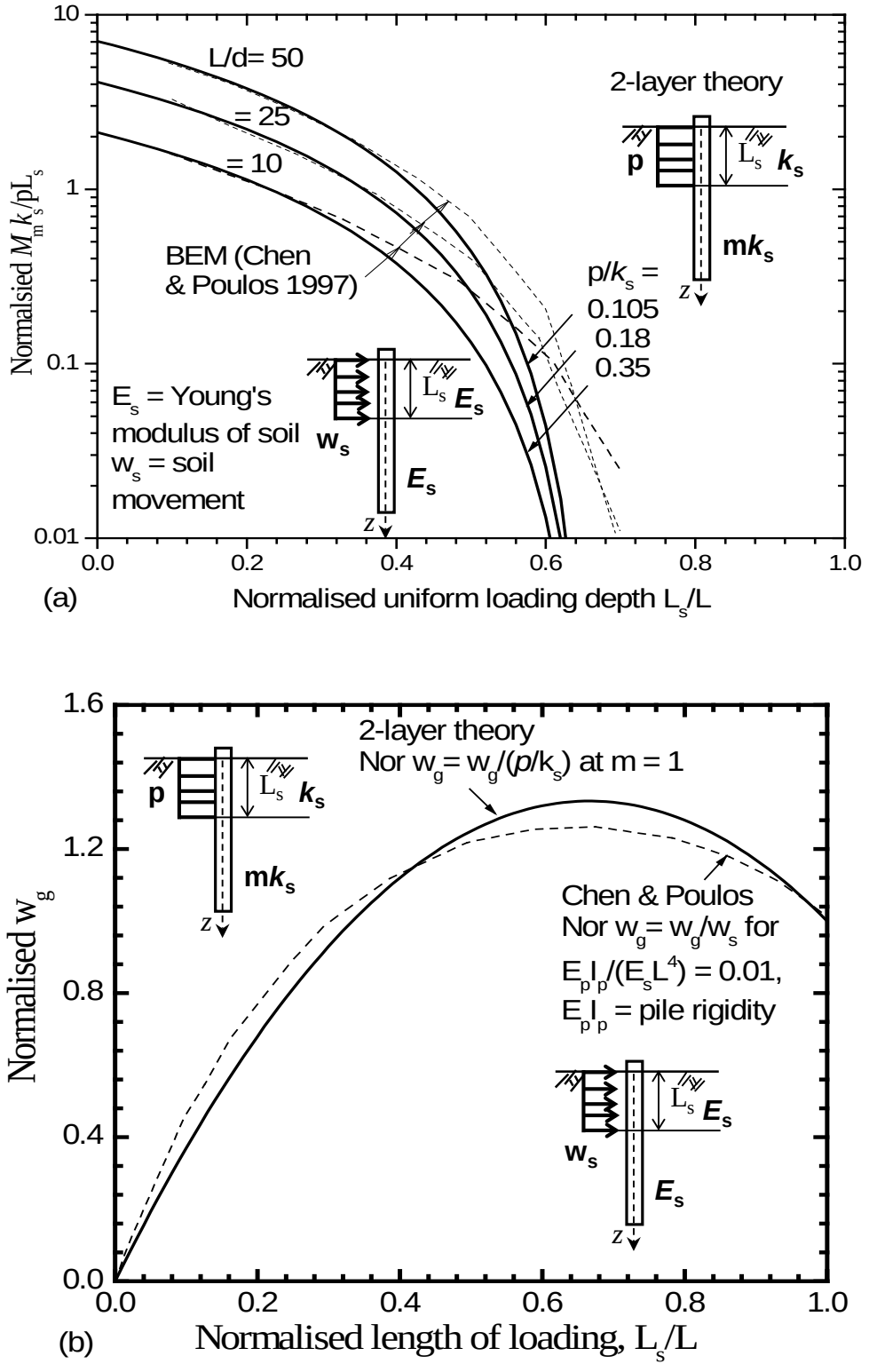

Figure 15 Comparison between current solution and BEM results [14] for uniform loading: (a) Normalized bending moment; (b) Normalized deflection

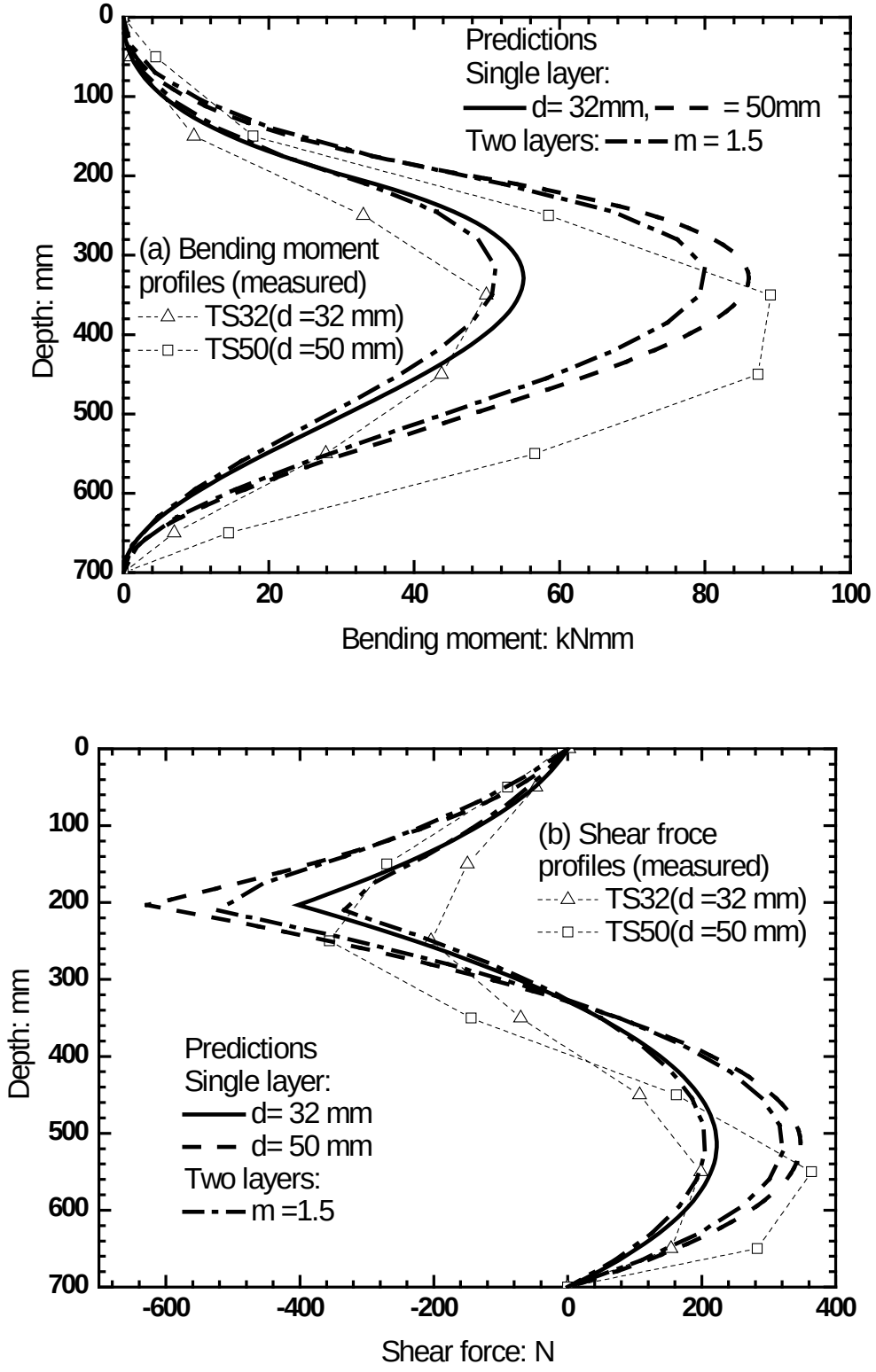

Figure 16. Predicted versus measured [5] response profiles of 2 tests (final sliding depth = 0.29*L*, and w/o axial load): (a) Bending moment; (b) Shear force

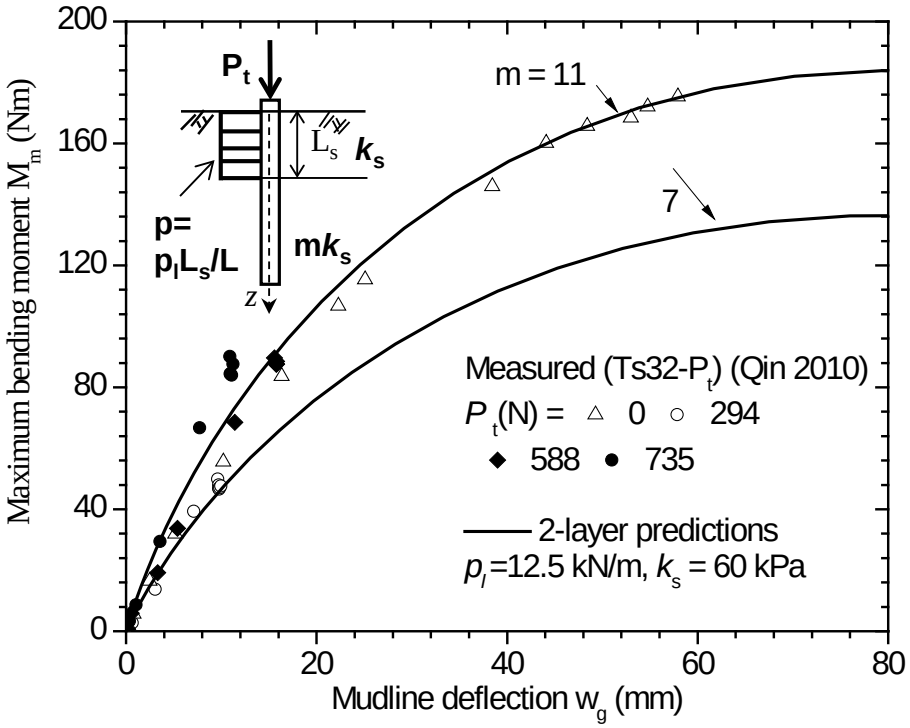

Figure 17 Comparison between 2-layer theory and the measured [15] curves of $w_g \sim M_m$ for passive piles with vertical loading

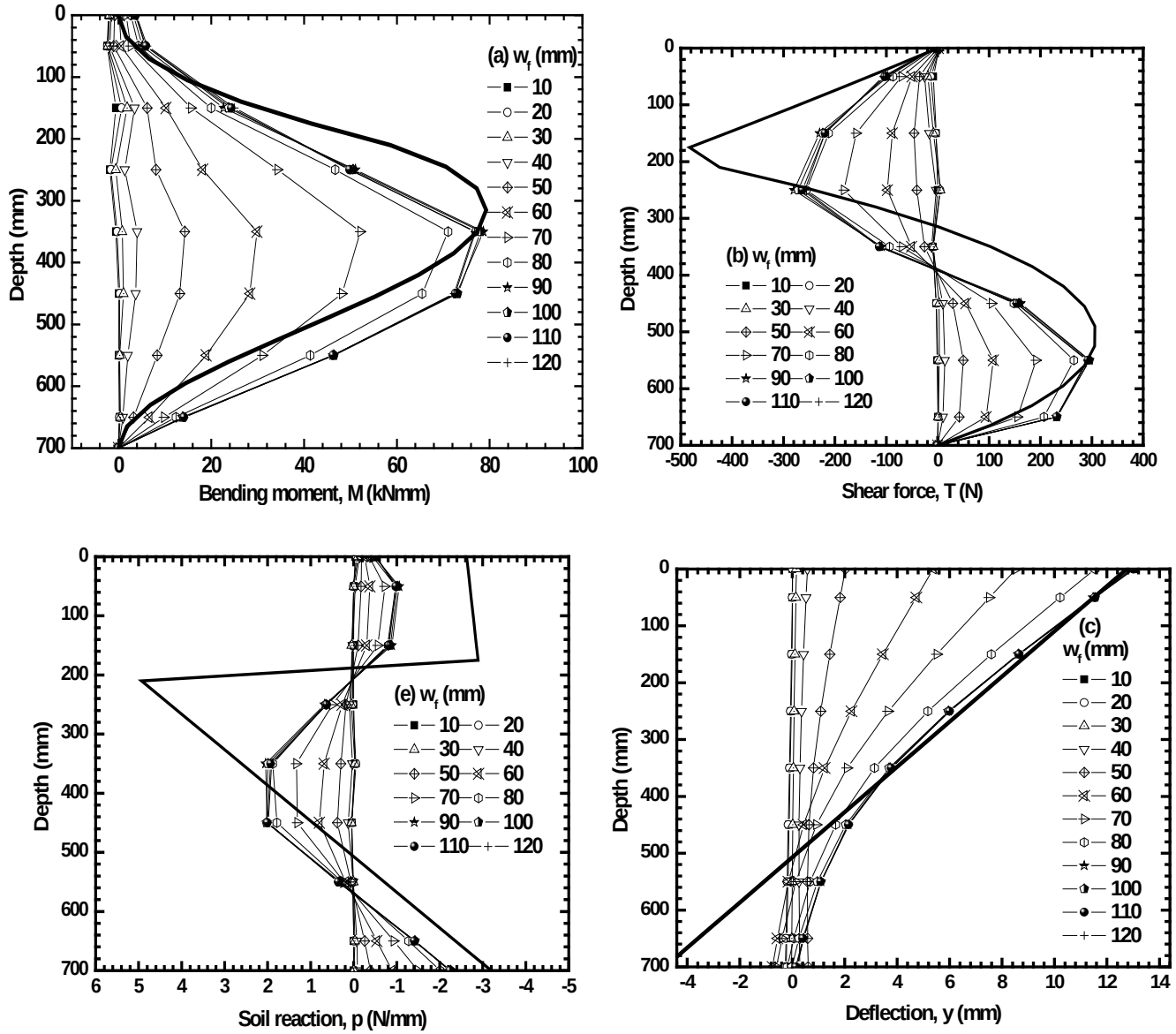

Figure 18 Response of pile duringTS32-294 (Prediction using m =11, L_s=190mm)